

A&A 602, A124 (2017)
 DOI: 10.1051/0004-6361/201629463
 © ESO 2017

**Astronomy
&
Astrophysics**

The nature of 50 Palermo *Swift*-BAT hard X-ray objects through optical spectroscopy[★]

A. F. Rojas¹, N. Masetti^{2,1}, D. Minniti^{1,3,4}, E. Jiménez-Bailón⁵, V. Chavushyan⁶, G. Hau⁷, V. A. McBride^{8,9}, L. Bassani², A. Bazzano¹⁰, A. J. Bird¹¹, G. Galaz¹², I. Gavignaud¹, R. Landi², A. Malizia², L. Morelli^{13,14}, E. Palazzi², V. Patiño-Álvarez^{15,6}, J. B. Stephen², and P. Ubertini¹⁰

¹ Departamento de Ciencias Físicas, Universidad Andrés Bello, Campus La Casona, Fernández Concha 700, Santiago, Chile
 e-mail: a.f.rojas@layu@gmail.com

² INAF – Istituto di Astrofisica Spaziale e Fisica Cosmica di Bologna, via Gobetti 101, 40129 Bologna, Italy

³ Millennium Institute of Astrophysics, Av. Vicuña Mackenna 4860, 782-0436 Macul, Santiago, Chile

⁴ Vatican Observatory, 00120 Vatican City State, Italy

⁵ Universidad Nacional Autónoma de México, Apartado Postal 70-264, 04510 México D.F., Mexico

⁶ Instituto Nacional de Astrofísica, Óptica y Electrónica, Apartado Postal 51-216, 72000 Puebla, Mexico

⁷ European Southern Observatory, Ave. Alonso de Cordoba 3107, Casilla 19001, Santiago, Chile

⁸ Department of Astronomy, Astrophysics, Cosmology and Gravity Centre, University of Cape Town, Private Bag X3, 7701 Rondebosch, South Africa

⁹ South African Astronomical Observatory, PO Box 9, 7935 Observatory, South Africa

¹⁰ INAF – Istituto di Astrofisica e Planetologia Spaziali, via Fosso del Cavaliere 100, 00133 Roma, Italy

¹¹ School of Physics & Astronomy, University of Southampton, Southampton, SO17 1BJ, UK

¹² Instituto de Astrofísica, Facultad de Física, Pontificia Universidad Católica de Chile, Casilla 306, Santiago 22, Chile

¹³ Dipartimento di Fisica ed Astronomia “G. Galilei”, Università di Padova, vicolo dell’Osservatorio 3, 35122 Padova, Italy

¹⁴ INAF-Osservatorio Astronomico di Padova, Vicolo dell’Osservatorio 5, 35122 Padova, Italy

¹⁵ Max-Planck-Institut für Radioastronomie, Auf dem Hügel 69, 53121 Bonn, Germany

Received 2 August 2016 / Accepted 5 February 2017

ABSTRACT

We present the nature of 50 hard X-ray emitting objects unveiled through an optical spectroscopy campaign performed at seven telescopes in the northern and southern hemispheres. These objects were detected with the Burst Alert Telescope (BAT) instrument onboard the *Swift* satellite and listed as of unidentified nature in the 54-month Palermo BAT catalogue. In detail, 45 sources in our sample are identified as active galactic nuclei of which, 27 are classified as type 1 (with broad and narrow emission lines) and 18 are classified as type 2 (with only narrow emission lines). Among the broad-line emission objects, one is a type 1 high-redshift quasi-stellar object, and among the narrow-line emission objects, one is a starburst galaxy, one is a X-ray bright optically normal galaxy, and one is a low ionization nuclear emission line region. We report 30 new redshift measurements, 13 confirmations and 2 more accurate redshift values. The remaining five objects are galactic sources: three are Cataclysmic Variables, one is a X-ray Binary probably with a low mass secondary star, and one is an active star.

Key words. galaxies: Seyfert – quasars: emission lines – X-rays: binaries – novae, cataclysmic variables – techniques: spectroscopic

1. Introduction

X-ray and γ -ray satellites have detected a large number of high energy sources, allowing us to explore and study in detail the hard X-ray band, above 15 keV. Specifically, the INTEGRAL (Winkler et al. 2003) and *Swift* (Gehrels et al. 2004) satellites are able to detect hard X-ray sources with positional accuracy better than 5 arcmin with their instruments IBIS (Ubertini et al. 2003) and BAT (Barthelmy 2004), respectively. There are more

than 1200 hard X-ray sources detected by these satellites, mostly active galactic nuclei (AGN, $\sim 60\%$) followed by X-ray binaries (XRBS, $\sim 15\%$), cataclysmic variables (CVs, $\sim 5\%$), and finally active stars (e.g. Baumgartner et al. 2013); but more than 20% of the whole set of detections has no precise classification or has no obvious counterpart at other wavelengths and therefore they cannot be associated with any known class of high-energy emitting objects.

Although the cross-correlation with catalogues of surveys at other wavelengths (soft X-ray, radio, or optical bands) is important for improving the positional accuracy of detected objects and pinpointing longer-wavelength candidate counterparts of these sources, only with the detection of emission spectral features especially in the optical can we confirm these associations and reveal the actual nature of these unclassified objects.

The identification and classification of these newly detected objects is important as it is useful, for instance, for binary system

[★] Based on observations obtained from the following observatories: Cerro Tololo Interamerican Observatory (Chile); Astronomical Observatory of Bologna in Loiano (Italy); Observatorio Astronómico Nacional (San Pedro Mártir, Mexico); Radcliffe telescope of the South African Astronomical Observatory (Sutherland, South Africa); Sloan Digital Sky Survey; Observatorio del Roque de los Muchachos of the Instituto de Astrofísica de Canarias (Canary Islands, Spain) and New Technology Telescope (NTT) of La Silla Observatory, Chile.

studies (Coleiro & Chaty 2013; Scaringi et al. 2010; Landi et al. 2009) and for population analysis of extragalactic objects (e.g. Ricci et al. 2015; Ajello et al. 2008). Moreover, one can find interesting classes of X-ray emitting objects, for example types of unusual AGN obscured by local absorption in their galaxies and Compton-thick AGNs with a line-of-sight hydrogen column $N_{\text{H}} > 10^{24} \text{ cm}^{-2}$ due to the torus of dust surrounding a supermassive black hole (Comastri et al. 2002; Malizia et al. 2009; Lutovinov et al. 2012; Baloković et al. 2014; Koss et al. 2016a; Ricci et al. 2015). Also, new types of hard X-ray binaries have been reported; namely, the INTEGRAL discovered supergiant fast X-ray transients (SFXTs, Sguera et al. 2006) and the γ -ray binary in de Martino et al. (2013). Due to local or Galactic absorption, many of these objects are optically faint, so one needs relatively large telescopes to identify their nature and get information about them, such as the study of stellar populations in their central regions (Morelli et al. 2013).

Many efforts have been made to characterise and analyse the properties of the *Swift*-BAT sample using optical spectroscopy (e.g. Landi et al. 2007; Winter et al. 2010; Berney et al. 2015; Halpern & Thorstensen 2015; Ueda et al. 2015), but the identification and precise classification of unassociated or poorly studied objects remains incomplete. The work presented here extends to fainter objects the work started in Parisi et al. (2009; 2012; 2014; hereafter PI, PII and PIII), and focuses on the identification and classification of unassociated hard X-ray sources detected by the BAT instrument onboard *Swift*, that are listed in the Second Palermo *Swift*-BAT Catalogue (2PBC, Cusumano et al. 2010).

The paper is structured as follows: in Sect. 2, we provide information about the sample selection; in Sect. 3, we describe the optical observations, telescopes employed, and reduction method used; in Sect. 4, the results of the optical classification of different classes (AGNs, XRBs, CVs and active stars) are presented and a statistical analysis of the sample is given; finally, in Sect. 5 we summarise the main conclusions of our work.

2. Sample selection

In this work we focus on the optical follow-up of objects with unknown classification and/or redshift that are reported in the Second Palermo *Swift*-BAT hard X-ray catalogue obtained by analysing data acquired in the first 54 months of the *Swift* mission (Cusumano et al. 2010).

This survey covers 90% of the sky down to a flux limit of $1.1 \times 10^{-11} \text{ erg cm}^{-2} \text{ s}^{-1}$ and 50% of the sky down to a flux limit of $0.9 \times 10^{-11} \text{ erg cm}^{-2} \text{ s}^{-1}$ in the 15–150 keV band. It lists 1256 sources, of which 57% are extragalactic, 19% are galactic, and 24% are of unknown type.

From this BAT survey, we selected a sample of unknown type objects and used the available soft X-ray data (<10 keV) to reduce the source positional uncertainty from arcmin to arcsec sized radii, using the ROSAT (Voges et al. 1999), *Swift*/XRT (0.3–10 keV, Evans et al. 2014), *XMM-Newton* (0.2–12 keV, Watson et al. 2009) catalogues or the *Chandra*¹ (0.3–10 keV, Aldcroft et al. 2000) and XRT² databases. This approach was proven by Stephen et al. (2006) to be very effective in associating hard X-ray sources with a strong, softer X-ray counterpart within the high-energy error circle with a high degree of probability, which in turn drastically reduces the positional error

¹ <http://cxc.harvard.edu>

² Agenzia spaziale italiana Science Data Center (ASDC): <http://asdc.asi.it>

Table 1. Observational information of finding charts of the soft X-ray counterpart identifications to the present sample of 2PBC sources.

Object	Obs date	Start time (UT)	Exposure time (s)
2PBC J0057.2+6401	Aug. 29, 2010	00:19:00	9807
2PBC J0116.5–1235	May 19, 2011	00:45:00	7372
2PBC J0128.5+1628	Jun. 04, 2009	01:33:00	10 643
2PBC J0154.1–5034	Nov. 14, 2012	00:29:00	2379
2PBC J0217.0–7250	Nov. 29, 2014	23:59:00	1743
2PBC J0252.3+4309	Mar. 28, 2011	10:54:00	4189
2PBC J0356.6–6252	Aug. 05, 2008	01:32:00	5659
2PBC J0440.6–6507	Nov. 18, 2012	16:38:00	4375
2PBC J0505.4–6734	Oct. 21, 2013	13:00:00	2071
2PBC J0550.7–2304	Nov. 27, 2012	07:23:00	3520
2PBC J0608.0+5749	Dec. 04, 2014	03:28:00	1093
2PBC J0620.8–2932	Jul. 03, 2013	00:14:00	4689
2PBC J0653.1–1227	Nov. 21, 2012	12:14:00	3139
2PBC J0709.5–3538	Jul. 23, 2013	16:58:02	2590
2PBC J0714.6–2521	Nov. 22, 2012	18:46:00	2724
2PBC J0751.6+6450	Feb. 28, 2013	05:04:00	1114
2PBC J0757.9+0113	Jun. 05, 2014	20:01:29	804
2PBC J0819.2–2508	Jul. 11, 2013	02:02:00	3814
2PBC J0838.7+2612	Dec. 22, 2013	11:25:41	2377
2PBC J1020.5–0235	Jul. 07, 2010	18:18:00	3144
2PBC J1042.2+0043	Jun. 25, 2010	09:12:50	7537
2PBC J1228.1–0925	Nov. 19, 2013	09:29:04	4173
2PBC J1332.1–7751	Feb. 26, 2009	08:49:00	9264
2PBC J1419.2+6804*	Jun. 11, 2005	17:27:54	9851
2PBC J1520.2–0433	Jan. 21, 2011	02:55:00	3344
2PBC J1548.5–3208	Feb. 01, 2009	00:23:06	2849
2PBC J1555.0–6225	Jul. 04, 2011	05:44:00	2430
2PBC J1649.3–1739	Sep. 07, 2010	00:19:21	2720
2PBC J1809.7–6555	Jul. 09, 2011	01:39:52	2979
2PBC J1832.8+3124	Jan. 27, 2014	06:06:00	3494
2PBC J1911.4+1412	Nov. 28, 2012	06:48:23	1239
2PBC J2029.4–6146	Jun. 20, 2010	00:03:21	6246
2PBC J2030.7–7530	Jul. 02, 2010	17:23:32	6547
2PBC J2045.9+8321	Jun. 18, 2010	01:11:42	5584
2PBC J2136.3+2003	Jun. 20, 2013	13:55:34	1573
2PBC J2155.1+6205	Jun. 23, 2013	02:25:26	4240
2PBC J2238.9+4050	Dec. 23, 2012	11:24:04	1556
2PBC J2322.6+2903	Nov. 11, 2012	01:45:09	4373
2PBC J2348.9+4153	Nov. 12, 2013	00:13:14	2275

Notes. Soft X-ray observations were obtained from ASI Science XRT database (<http://www.asdc.asi.it/>). (*) Soft X-ray observation from HEASARC database (<http://heasarc.gsfc.nasa.gov>).

circles to a few arcsec in radius, thus shrinking the search area by a factor of $\sim 10^4$.

More specifically, for the present sample, we analysed the soft X-ray (<10 keV) images with longest available exposure of the field of each BAT object in Table 1 to search for sources detected (at confidence level $>3\sigma$) within the 90% *Swift*-BAT error circles. This choice also allowed us to investigate the source hardness in case of multiple objects within the hard X-ray error box, which permitted us to pinpoint the hardest sources, hence the most likely counterparts to the BAT objects.

Nearly all soft X-ray images were extracted from the ASDC XRT database (see footnote 2); that of 2PBC J1419.2+6804 was instead obtained from an *XMM-Newton* observation downloaded from the HEASARC database³. The information about these images can be found in Table 1 and the coordinates of the most likely counterparts are reported in Table 2 (second and

³ <http://heasarc.gsfc.nasa.gov>

third columns) together with their relative uncertainties (fourth column).

In most of the cases, that is for 33 objects, we found a single bright soft X-ray object within the BAT 90% confidence level error box with emission above 3 keV, and the soft X-ray counterpart positions of these BAT objects are provided in Fig. A.1, where for each image the BAT error circle is shown in blue and the black arrow indicates the soft X-ray counterpart for which the optical spectra were acquired. On the other hand, we found that 11 of the proposed soft X-ray counterparts to BAT objects in this paper are coincident with the proposed ROSAT or XRT counterpart reported in the Cusumano et al. (2010) and/or Baumgartner et al. (2013) catalogues. We list them in Table 2.

For the remaining six objects we needed to consider additional criteria as we detail below.

When no soft X-ray counterpart was found inside the BAT error circle at 90% position confidence level, we expanded the search area by considering the 99% BAT error circle assuming a gaussian uncertainty distribution for the error radius. In our sample, the putative counterparts of three objects were selected considering the 99% BAT error circle: those of 2PBC J0550.7–2304, 2PBC J0620.8–2932, and 2PBC J1832.8+3124. Since no other object is detected inside the 99% positional uncertainty, we assumed these associations to be correct (see Fig. A.2). We remark here that the soft X-ray counterpart indicated with the black arrow for the object 2PBC J0550.7–2304 corresponds to the ROSAT object proposed as a soft X-ray counterpart in the Cusumano et al. (2010) catalogue and lies at the edge of the 99% BAT error circle.

In one single case, we included in our sample an object reported by PIII and for which no soft X-ray counterpart was found within its 99% BAT error circle. Actually, PIII found two nearby soft X-ray sources as possible associations of the object PBC J1020.5–0235, which are the same sources labelled as Swift J1020.5–0237A and Swift J1020.5–0237B in the 70-month BAT Catalogue of Baumgartner et al. (2013). In PIII the object with higher 3–10 keV flux was considered for optical spectroscopy (object B) and identified as Sy 1 galaxy at $z = 0.060$. We thus decided to complete the information about this field by analysing the optical spectrum of the object Swift J1020.5–0237A (see Fig. A.3).

Finally for two cases, 2PBC J0819.2–2508 and 2PBC J1520.2–0433, the soft X-ray counterparts proposed in this work do not coincide with those reported in the Cusumano et al. (2010) and/or Baumgartner et al. (2013) catalogues (see Fig. A.4).

Then, within the soft X-ray error boxes of each source of our sample, we identified the putative optical counterpart(s) to the BAT object and performed optical spectroscopic follow-up work with long-slit spectroscopy. Following the method applied by Masetti et al. (2004, 2006a,b,c,d, 2008, 2009, 2010, 2012, 2013, hereafter MI to MX respectively) and by PI, PII, and PIII, we determined the nature of 50 selected objects, estimating also redshifts, distances, Galactic and local extinction, and central black hole masses for type 1 AGNs. The observational information of the 50 objects are listed in Table 2.

3. Optical observations

The data presented in this work involved the use of the following telescopes:

- the 1.5 m at the Cerro Tololo Interamerican Observatory (CTIO), Chile;

- the 1.52 m *Cassini* telescope of the Astronomical Observatory of Bologna, in Loiano, Italy;
- the 2.1 m telescope of the Observatorio Astronómico Nacional in San Pedro Mártir (SPM), Mexico;
- the 3.58 m Telescopio Nazionale *Galileo* (TNG) at the Roque de Los Muchachos Observatory in La Palma, Spain;
- the 1.9 m Radcliffe telescope of the South African Astronomical Observatory (Sutherland, South Africa);
- the 2.5 m SDSS at the Apache Point Observatory (APO), Sunspot, New Mexico;
- the 3.5 m New Technology Telescope (NTT) of La Silla Observatory, Chile.

In Table 2, we show a detailed log of all the spectroscopic observations presented in this work. Column 1 indicates the names of the observed 2PBC sources. In Cols. 2 and 3, we list the soft X-ray coordinates of the proposed counterpart (with their respective positional uncertainties in Col. 4) extracted from the *XMM-Newton* (with an uncertainty better than 2", Watson et al. 2009) and the XRT catalogues (with an uncertainty of $\sim 6''$ for the PC interactive mode according to Evans et al. 2014). In Cols. 5 and 6, we list the equatorial coordinates of the proposed counterpart, mostly extracted from the 2MASS (with an uncertainty of 0".1: Skrutskie et al. 2006) or USNO-A2.0 catalogues (with an uncertainty of 0".2, Deutsch 1999; Assafin et al. 2001).

The telescope and instrument used for the observations are reported in Col. 7, while the main characteristics of each spectroscopic setup are presented in Cols. 8–10. Column 11 reports the observation date and the UT time at mid-exposure, and Col. 12 provides the exposure times and the number of observations for each source.

The instrumental resolutions (in Å) for the different setups of the optical spectra presented here are listed in Tables 2 and 3. The spectroscopic data acquired have been extracted (Horne 1986) and reduced following standard procedures using IRAF⁴. Calibration frames (flat fields and bias) were taken on the day preceding or following the observing night. The wavelength calibration was performed using lamp data acquired soon after each on-target spectroscopic acquisition; the uncertainty in this calibration was ~ 0.5 Å in all cases according to our checks that used the positions of background night sky lines. Flux calibration was obtained using catalogued spectrophotometric standards. Finally, the data of a given object were stacked together to increase the signal-to-noise ratio when multiple spectra were acquired. The Sloan Digital Sky Survey (SDSS) spectrum of 2PBC J0838.7+2612 was acquired from the corresponding online archive⁵, already reduced and calibrated.

4. Results

The spectra of 50 objects were analysed according to the above steps. Of these, 45 were classified as extragalactic objects and the remaining five objects presented features in their spectra consistent with those of galactic sources.

The main criteria used for the classification of the extragalactic sources spectra are reported hereafter. We assume a cosmology with $H_0 = 70$ km s⁻¹ Mpc⁻¹, $\Omega_\Lambda = 0.7$, and $\Omega_m = 0.3$; the luminosity distances of the extragalactic objects presented in this

⁴ IRAF is the Image Reduction and Analysis Facility made available to the astronomical community by the National Optical Astronomy Observatories, which are operated by AURA, Inc., under contract with the US National Science Foundation. It is available at <http://iraf.noao.edu/>

⁵ <http://www.sdss.org>

Table 2. Log of the spectroscopic observations presented in this paper (see text for details).

(1) Object	(2) RA X-ray (J2000)	(3) Dec X-ray (J2000)	(4) Error radius (arcsec)	(5) RA opt. (J2000)	(6) Dec opt. (J2000)	(7) Telescope+instrument	(8) λ range (Å)	(9) Disp. (Å/pix)	(10) Resolution <i>FWHM</i> (Å)	(11) UT date and time at mid-exposure	(12) Exposure time (s)
2PBC J0057.2+6401 ^A	00:57:12.77	+63:59:41.3	3.6	00:57:12.85	+63:59:42.9	TNG+DOLoReS	3700–8000	2.5	10	02 Aug. 2011, 04:48	2 × 1200
2PBC J0116.5–1235 ^A	01:16:31.05	–12:36:19.0	3.5	01:16:31.14	–12:36:17.0	TNG+DOLoReS	3700–8000	2.5	15	19 Aug. 2011, 04:29	2 × 900
2PBC J0128.5+1628 ^A	01:28:24.46	+16:27:30.4	3.9	01:28:24.45	+16:27:33.5	SPM 2.1 m+B&C Spec.	3300–7900	4.0	18	28 Sep. 2011, 07:36	2 × 1800
2PBC J0154.1–5034	01:53:50.90	–50:31:36.8	6.0	01:53:51.51	–50:31:37.7	NTT+EFOSC2	3685–9315	2.8	21	29 Aug. 2015, 06:30	2 × 600
2PBC J0217.0–7250	02:17:36.10	–72:51:27.7	6.0	02:17:35.72	–72:51:28.1	NTT+EFOSC2	3685–9315	2.8	21	28 Aug. 2015, 10:09	2 × 300
2PBC J0252.3+4309 ^A	02:52:34.02	+43:10:01.8	4.1	02:52:34.02	+43:10:02.8	SPM 2.1 m+B&C Spec.	3300–7900	4.0	18	29 Sep. 2011, 09:04	2 × 1800
2PBC J0356.6–6252 ^A	03:56:19.66	–62:51:36.6	4.1	03:56:19.97	–62:51:39.1	CTIO 1.5 m+RC Spec.	3300–10 500	5.7	14	24 Sep. 2011, 05:40	2 × 1800
2PBC J0440.6–6507	04:40:35.30	–65:07:50.8	6.0	04:40:35.63	–65:07:48.7	NTT+EFOSC2	3685–9315	2.8	21	29 Aug. 2015, 06:57	2 × 600
2PBC J0505.4–6734 ^A	05:05:24.33 [*]	–67:34:35.5 [*]	2.0	05:05:24.50 ^U	–67:34:36.2 ^U	CTIO 1.5 m+RC Spec.	3300–10 500	5.7	14	24 Sep. 2011, 07:34	2 × 1500
2PBC J0550.7–2304 [‡]	05:50:39.10	–23:11:16.4	6.0	05:50:39.51	–23:11:17.7	CTIO 1.5 m+RC Spec.	3300–10 500	5.7	14	02 Oct. 2011, 08:40	2 × 400
2PBC J0608.0+5749	06:08:09.40	+57:51:07.9	6.0	06:08:09.67	+57:51:04.5	SPM 2.1 m+B&C Spec.	3300–7900	4.0	18	27 Feb. 2015, 04:09	3 × 1200
2PBC J0620.8–2932 ^{‡,‡}	06:20:59.90	–29:27:31.6	6.0	06:21:00.05	–29:27:34.6	SPM 2.1 m+B&C Spec.	3300–7900	4.0	18	04 Dec. 2013, 08:37	1200+900
2PBC J0640.1–4740 ^A	06:40:13.46	–47:41:33.4	3.9	06:40:13.53	–47:41:34.3	CTIO 1.5 m+RC Spec.	3300–10 500	5.7	14	17 Nov. 2011, 04:43	2 × 1800
(=Swift J064013.50–474132.9)											
2PBC J0653.1–1227	06:53:16.40	–12:29:37.3	6.0	06:53:16.60 ^U	–12:29:37.0 ^U	TNG+DOLoReS	3700–8000	2.5	15	03 Feb. 2013, 22:55	2 × 1800
2PBC J0658.0–1746	06:58:06.08	–17:44:21.0	3.6	06:58:05.87 ^U	–17:44:16.3 ^U	Radcliffe+Gr. Spec.	3750–7750	2.3	6	20 Nov. 2011, 07:20	1310
(=1RXS J065806.3–174427)											
2PBC J0709.5–3538	07:09:31.80	–35:37:46.2	6.0	07:09:32.05	–35:37:46.4	SPM 2.1 m+B&C Spec.	3300–7900	4.0	18	05 Dec. 2013, 11:00	2 × 1800
2PBC J0714.6–2521 ^A	07:14:37.10	–25:17:22.9	6.0	07:14:36.98	–25:17:25.2	TNG+DOLoReS	3700–8000	2.5	15	04 Feb. 2013, 00:38	2 × 1200
2PBC J0717.8–2156 ^A	07:17:48.28	–21:53:03.0	3.6	07:17:48.28 ^U	–21:53:05.1 ^U	TNG+DOLoReS	3700–8000	2.5	20	22 Oct. 2012, 04:11	1200
(=1RXS J071748.9–215306)											
2PBC J0751.6+6450	07:51:44.70	+64:48:59.7	6.0	07:51:45.41	+64:49:03.7	Cassini+BFOSC	3500–8700	4.0	12	21 Mar. 2013, 21:37	1800
2PBC J0757.9+0113	07:57:44.10	+01:13:42.9	6.0	07:57:44.00	+01:13:42.7	TNG+DOLoReS	3700–8000	2.5	15	04 Jan. 2014, 00:24	2 × 1200
2PBC J0800.5–4306 ^{A,‡}	08:00:39.99	–43:11:06.4	3.5	08:00:39.98	–43:11:07.6	CTIO 1.5m+RC Spec.	3300–10 500	5.7	14	07 Dec. 2011, 03:48	2 × 1800
(=Swift J080040.2–431107)											
2PBC J0812.3–4003 ^A	08:12:14.16	–40:03:23.7	3.5	08:12:14.01	–40:03:23.9	CTIO 1.5m+RC Spec.	3300–10 500	5.7	14	24 Nov. 2011, 06:58	3 × 1800
(=1RXS J081215.2–400336)											
2PBC J0819.2–2508	08:19:14.80	–25:11:17.1	6.0	08:19:14.74	–25:11:16.6	CTIO 1.5m+RC Spec.	3300–10 500	5.7	14	17 Nov. 2011, 05:45	2 × 1000
2PBC J0838.7+2612	08:38:57.00	+26:10:37.5	6.0	08:38:56.88	+26:10:37.5	SDSS+CCD Spc.	3800–9200	1.0	3	08 Dec. 2004, 00:00	4300
2PBC J0854.3–0826 ^A	08:54:29.20	–08:24:28.6	2.7	08:54:29.27	–08:24:27.6	TNG+DOLoReS	3700–8000	2.5	15	01 Dec. 2011, 02:41	2 × 900
(=Swift J085429.35–082428.6)											
2PBC J1020.5–0235 ^{A,‡}	10:21:02.90	–02:36:46.0	6.0	10:21:03.09 ^U	–02:36:42.6 ^U	TNG+DOLoReS	3700–8000	2.5	15	04 Jan. 2014, 05:34	2 × 1200
2PBC J1042.2+0043 ^A	10:42:08.33	+00:42:06.8	3.6	10:42:08.36	+00:42:06.0	TNG+DOLoReS	3700–8000	2.5	20	23 Feb. 2012, 05:40	2 × 1500
2PBC J1228.1–0925	12:28:10.00	–09:27:03.9	6.0	12:28:10.14	–09:27:03.5	SPM 2.1 m+B&C Spec.	3300–7900	4.0	18	26 Feb. 2015, 11:18	2 × 1800
2PBC J1251.8–5127	12:51:44.04	–51:28:04.3	3.6	12:51:44.07	–51:28:05.2	CTIO 1.5 m+RC Spec.	3300–10 500	5.7	14	22 Dec. 2011, 08:28	1620
(=1RXS J125144.2–512809)											
2PBC J1332.1–7751 ^A	13:32:40.64	–77:50:39.0	4.1	13:32:40.59	–77:50:40.5	CTIO 1.5 m+RC Spec.	3300–10 500	5.7	14	03 Feb. 2012, 07:52	2 × 1000
2PBC J1419.2+6804	14:18:49.94 [*]	+68:04:09.9	2.0	14:18:49.91	+68:04:09.7	Cassini+BFOSC	3500–8700	4.0	12	26 Feb. 2012, 02:00	2 × 1800
2PBC J1520.2–0433	15:20:14.98	–04:35:52.6	3.6	15:20:15.07	–04:35:53.0	Cassini+BFOSC	3500–8700	4.0	12	12 Apr. 2015, 01:25	2 × 1800
2PBC J1548.5–3208	15:48:43.35	–32:07:11.0	2.7	15:48:43.39	–32:07:13.3	CTIO 1.5m+RC Spec.	3300–10 500	5.7	14	05 Apr. 2012, 08:22	2 × 1500
2PBC J1555.0–6225	15:54:59.25	–62:24:30.0	4.2	15:54:58.95	–62:24:28.3	CTIO 1.5 m+RC Spec.	3300–10 500	5.7	14	19 May. 2012, 07:14	2 × 1500
2PBC J1649.3–1739	16:49:20.92	–17:38:40.7	3.6	16:49:21.02	–17:38:40.6	SPM 2.1 m+B&C Spec.	3300–7900	4.0	18	22 Jun. 2012, 06:34	2 × 1800
2PBC J1709.7–2349	17:09:44.69 [*]	–23:46:53.1 [*]	2.0	17:09:44.70	–23:46:53.2	SPM 2.1 m+B&C Spec.	3300–7900	4.0	18	25 Jun. 2012, 05:59	2 × 1200
(=1RXS J170944.9–234658)											
2PBC J1742.0–6053 ^A	17:42:01.74	–60:55:13.6	3.5	17:42:01.50	–60:55:12.2	CTIO 1.5 m+RC Spec.	3300–10 500	5.7	14	26 Oct. 2011, 00:24	2 × 1200
(=1RXS J174201.5–605514)											
2PBC J1809.7–6555	18:09:52.19	–65:56:11.9	3.5	18:09:52.28	–65:56:13.8	CTIO 1.5 m+RC Spec.	3300–10 500	5.7	14	08 Oct. 2011, 02:32	2 × 1800
2PBC J1832.8+3124 [‡]	18:32:26.20	+31:29:04.2	6.0	18:32:26.19	+31:29:04.8	TNG+DOLoReS	3700–8000	2.5	15	04 May. 2014, 02:00	3 × 1200
2PBC J1911.4+1412	19:11:24.70	+14:11:44.8	6.0	19:11:24.87 ^U	+14:11:44.9 ^U	TNG+DOLoReS	3700–8000	2.5	15	11 Apr. 2013, 03:20	2 × 1800
2PBC J2010.3–2522 ^A	20:10:19.74	–25:23:59.8	3.6	20:10:19.76 ^U	–25:23:59.4 ^U	TNG+DOLoReS	3700–8000	2.5	15	20 Jun. 2012, 04:56	2 × 1800
(=1RXS J201020.0–252356)											
2PBC J2029.4–6146 ^A	20:29:31.08	–61:49:07.7	3.6	20:29:31.23	–61:49:08.7	CTIO 1.5 m+RC Spec.	3300–10 500	5.7	14	22 Aug. 2011, 06:09	2 × 600
2PBC J2030.7–7530 ^A	20:30:41.80	–75:32:41.2	3.6	20:30:41.71	–75:32:43.0	CTIO 1.5 m+RC Spec.	3300–10 500	5.7	14	22 Aug. 2011, 05:14	2 × 1800
2PBC J2045.9+8321	20:44:13.29	+83:19:40.1	3.6	20:44:14.22 ^U	+83:19:42.4 ^U	TNG+DOLoReS	3700–8000	2.5	15	04 Aug. 2011, 02:14	2 × 1200
2PBC J2048.3+3812 ^A	20:48:27.08	+38:11:23.5	3.6	20:48:27.06	+38:11:24.5	TNG+DOLoReS	3700–8000	2.5	15	04 Aug. 2011, 01:09	2 × 1800
(=1RXS J204826.8+381120)											
2PBC J2136.3+2003	21:36:15.10	+20:02:03.4	6.0	21:36:15.31	+20:02:07.2	SPM 2.1 m+B&C Spec.	3300–7900	4.0	18	12 Jun. 2013, 08:58	2 × 1800
2PBC J2155.1+6205	21:55:15.30	+62:06:50.0	6.0	21:55:15.37	+62:06:46.4	TNG+DOLoReS	3700–8000	2.5	15	19 Sep. 2013, 04:56	2 × 1200
2PBC J2238.9+4050	22:38:56.50	+40:51:38.5	6.0	22:38:57.02	+40:51:42.0	Cassini+BFOSC	3500–8700	4.0	12	05 Nov. 2013, 21:40	2 × 1800
2PBC J2322.6+2903	23:22:45.70	+29:08:12.8	6.0	23:22:45.86	+29:08:16.2	Cassini+BFOSC	3500–8700	4.0	12	03 Dec. 2012, 17:52	2 × 1800
2PBC J2348.9+4153 [°]	23:48:53.80	+41:54:28.0	6.0	23:48:53.46	+41:54:28.6	SPM 2.1 m+B&C Spec.	3300–7900	4.0	18	06 Dec. 2013, 03:19	2 × 1800

Notes. If not indicated otherwise, soft X-ray source coordinates were extracted from XRT (<http://www.swift.ac.uk/1SXPS/> or interactive mode (°) in <http://www.asdc.asi.it/mmia/index.php?mission=swiftmastr>, with an accuracy $\sim 6''$) or from *XMM-Newton* observations (°) with an accuracy better than $2''$. Coordinates from the 2MASS catalogue have an accuracy better than $0''.1$ whereas from USNO-A2.0 catalogue (°) have an accuracy of about $0''.2$. (°) Sources for which the 99% BAT error circle was considered to search for a soft X-ray counterpart. (°) Source outside the corresponding 99% XRT error circle. (°) Proposed soft X-ray counterpart with no detected emission above 3 keV. (°) Object listed also in the 70-month *Swift*-BAT catalogue (Baumgartner et al. 2013). (°) Object listed also in the IBIS soft γ -ray sky after 1000 INTEGRAL orbits (Baumgartner et al. 2016).

Table 3. Instrumental setups of the telescopes used to gather the observations presented in this paper.

Telescope	Instrument	Grating	Slit width ($''$)	Resolution $FWHM$ (\AA)
TNG	LRS	LR-B	1.0	10
			1.5	15
			2.0	20
SPM	B&C	300	2.5	18
NTT	EFOSC2	Gr13	1.0	21
CTIO 1.5 m	R-C	13/I	1.5	14
SAAO 1.9 m	300	Gr7	2.0	6
SDSS	SDSS Spec.	Blue+Red	2.3	3
<i>Cassini</i>	BFOSC	Gr4	2.0	12

paper were determined for these parameters using the cosmology calculator of [Wright \(2006\)](#).

In order to distinguish between type 1 and type 2 emission-line AGN, we used the criteria of [Veilleux & Osterbrock \(1987\)](#) and we used the line ratio diagnostics of [Ho et al. \(1993, 1997\)](#) and [Kauffmann et al. \(2003\)](#) to distinguish among the Seyfert 2, low-ionization nuclear emission-line regions (LINERs; [Heckman 1980](#)), HII regions, and transition objects (LINERs whose integrated spectra are diluted or contaminated by neighbouring HII regions, [Ho et al. 1997](#)). For the subclass assignment to Seyfert 1 galaxies, we used the $H_{\beta}/[OIII]\lambda 5007$ line flux ratio criterion of [Winkler \(1992\)](#).

To estimate the $E(B-V)$ local optical absorption in our type 2 AGN sample, when possible, we first dereddened the spectrum by applying a correction for the Galactic absorption along the line of sight to the source. This was done using the galactic colour excess $E(B-V)_{\text{Gal}}$ given by [Schlegel et al. \(1998\)](#) and the Galactic extinction law obtained by [Cardelli et al. \(1989\)](#). We then estimated the colour excess $E(B-V)_{\text{AGN}}$ local to the AGN host galaxy by using the resulting $\frac{F_{H\alpha}}{F_{H\beta}}$ line ratio and corrected that assuming a Milky Way reddening using the Balmer decrement flux relation of [Osterbrock \(1989\)](#) that for normal density and temperature conditions implies $\left(\frac{F_{H\alpha}}{F_{H\beta}}\right)_* = 2.86$.

For most of our type 1 AGN sample we also estimated the mass of the central black hole. We generally used the H_{β} emission line flux, corrected for the Galactic colour excess ([Schlegel et al. 1998](#)) and its full width half maximum (FWHM) to measure the broad-line region (BLR) gas velocity (v_{FWHM}). Using Eq. (2) of [Wu et al. \(2004\)](#), we estimated the BLR size, which is used with v_{FWHM} in Eq. (5) of [Kaspi et al. \(2000\)](#) to calculate the AGNs black hole mass. For the single quasi-stellar object (QSO) of our sample, we apply the formulae from [McLure & Jarvis \(2002\)](#), which use the information afforded by the Mg II broad emission. As already remarked in our previous papers, the main sources of error in these mass estimates generally come from the determination of the flux of the employed emission lines, which is $\sim 15\%$ in the sample, and from the scatter in the scaling relation between the size of the BLR and the diagnostic line luminosity ([Vestergaard 2004](#)). Therefore, we expect the typical error to be around 50% of the black hole mass value.

The results of the black hole (BH) masses determination are reported in Sect. 4.4 where we also list the Eddington luminosities which were computed using the observed X-ray fluxes or upper limits in the 15–150 keV band and the median bolometric correction according to [Ho \(2009\)](#). For that, we first converted the observed X-ray luminosity measured in the *Swift*-BAT

survey in the energy range 15–150 keV to the intrinsic 2–10 keV luminosity ($L_{2-10 \text{ keV}}$) by dividing by 2.67 following [Rigby et al. \(2009\)](#) and [Marconi et al. \(2004\)](#), and then we applied the bolometric correction factor of $C_X = 15.8$ between the bolometric luminosity (L_{BOL}) and the X-ray luminosity in the 2–10 keV band according to [Ho \(2009\)](#). We would like to stress that our estimation of the bolometric luminosity implies an approximation because [Rigby et al. \(2009\)](#) and [Marconi et al. \(2004\)](#) used a conversion from 14–195 keV to 2–10 keV energy band whereas our reference hard X-ray band is 15–150 keV.

To evaluate the distances of the compact Galactic X-ray sources of our sample, we assumed an absolute magnitude $M_V \sim +9$ and an intrinsic colour index $(V-R)_0 \sim 0$ mag ([Warner 1995](#)) for CVs, whereas we assumed $M_V \sim 0$ and $(V-R)_0 \sim 0$ for the X-ray binary ([van Paradijs & McClintock 1995](#)). Although these approaches basically provide an approximate value for the distance of Galactic sources, our past experience (MI-X and PI-III) tells us that these estimates can be considered correct to within 50% of the refined value subsequently determined with more precise approaches. The values for the absorption in the optical V band along the line of sight of the galactic objects for the determination of distances were again estimated from the H_{α}/H_{β} flux ratio following [Osterbrock \(1989\)](#).

The X-ray luminosities reported in Tables 4 to 7, D.1 and D.2 are associated with a letter indicating the satellite and/or the instrument, namely the *Swift*-BAT (C) from [Cusumano et al. \(2010\)](#), *Swift*-BAT (B) from [Baumgartner et al. \(2013\)](#), and INTEGRAL/IBIS (I) from [Baumgartner et al. \(2016\)](#) catalogues, and from the *Swift*/XRT (X) and *XMM-Newton* (N) databases, with which the measurement of the corresponding X-ray flux was obtained. For the cases in which the soft X-ray information was obtained from the ASDC⁶ archive, we derived the 0.3–10 keV flux by assuming a power law model with photon index $\Gamma = 1.8$ and N_H value formulated by [Predehl & Schmitt \(1995\)](#) according to [Schlegel et al. \(1998\)](#) using the webpimms tool⁷ in order to obtain their soft X-ray luminosities.

For galactic objects with a soft X-ray counterpart from the ASDC archive, we assumed different spectral models according to their nature in order to obtain their soft X-ray fluxes. Specifically, for the probable X-ray binary 2PBC J1911.4+1412 we considered a power law model with $\Gamma = 2.1$, that is, a Crab-like spectrum, and for the active star 2PBC J0620.8–2932 we assumed a black body model with a typical value for these objects of $kT = 1$ keV ([Pandey et al. 2005](#)).

In the following, we present the object identifications by dividing them into four broad classes (X-ray binaries, CVs, active stars, and AGNs).

4.1. 2PBC J1911.4+1412: an X-ray binary?

Among the objects in our sample, 2PBC J1911.4+1412 displays optical features of an X-ray binary (see Fig. 1).

In the optical spectrum of this source, we detected emissions of Balmer lines up to H_{δ} and emission of He I at a redshift consistent with 0 superimposed on a reddened continuum. Moreover, the spectrum displays an emission of He II $_{\lambda 4686}$, typical of accretion disks. Table 4 lists the relevant optical spectral information along with the main parameters determined from available X-ray and optical data. The value for the absorption in the optical along the line of sight reported in that Table for the object is lower than

⁶ <http://www.asdc.asi.it/>

⁷ <https://heasarc.gsfc.nasa.gov/cgi-bin/Tools/w3pimms/w3pimms.pl>.

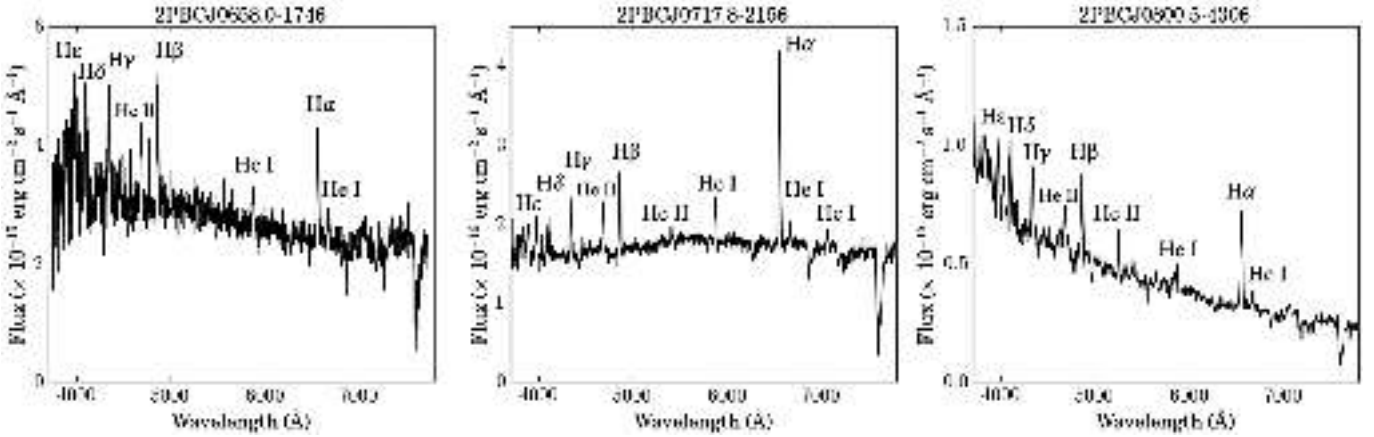


Fig. 2. Spectra (not corrected for the intervening Galactic absorption) of the optical counterparts of the three CVs belonging to the sample of BAT sources presented in this paper. For each spectrum, the main spectral features are labelled and \oplus indicates telluric absorptions.

Table 5. Synoptic table containing the main results concerning the three CVs identified in the present sample of 2PBC sources.

Object	H_{α}		H_{β}		He II $\lambda 4686$		R mag	d (pc)	L_X
	EW	Flux	EW	Flux	EW	Flux			
2PBC J0658.0–1746	20 ± 2	48 ± 3	19 ± 2	55 ± 3	10 ± 1	31 ± 4	15.4	~ 190	$3.4 (15-150)^C$ $8.1 (0.3-10)^X$
2PBC J0717.8–2156	30.6 ± 1.4	5.20 ± 0.15	12.7 ± 0.4	1.9 ± 0.1	8.3 ± 0.2	1.3 ± 0.1	16.1	~ 260	$4.9 (15-150)^C$ $2.8 (0.3-10)^X$ $6.4 (14-195)^B$
2PBC J0800.5–4306	34 ± 3	10.7 ± 0.4	18.8 ± 2.3	9.5 ± 0.4	24 ± 9	13 ± 4	16.8	~ 360	$12.4 (15-150)^C$ $9.6 (0.3-10)^X$ $5.8 (20-40)^I$ $10.1 (14-195)^B$

Notes. EWs are expressed in \AA , line fluxes are in units of $10^{-15} \text{ erg cm}^{-2} \text{ s}^{-1}$, X-ray luminosities are in units of $10^{31} \text{ erg s}^{-1}$, and the reference band (between round brackets) is expressed in keV. In the last column, the upper case letter indicates the satellite and/or the instrument with which the corresponding X-ray flux measurement was obtained (see text). ^(C) From *Swift*-BAT catalogue (Cusumano et al. 2010), ^(X) from *Swift*/XRT, ^(B) from *Swift*-BAT (Baumgartner et al. 2013) and ^(I) from INTEGRAL/IBIS catalogue (Baumgartner et al. 2016).

4.3. Active stars

The object 2PBC J0620.8–2932 shows the optical features of an active star in its spectrum (Fig. 3). We recall that this object is within the BAT error box at 99% confidence level and does not display X-ray emission at above 3 keV in the XRT observations; nevertheless, we suggest that this source can be classified as a chromospherically active star, with a star-like continuum typical of late-G/early-K type stars, a faint emission of H_{α} , and absorption bands such as G, NaD, and Mg b at $z = 0$, and we think that the flux above 3 keV from this source is possibly transient and could be due to flares (Sguera et al. 2016; Krivonos et al. 2007; MVI; MIX; MX). This conclusion is supported by the comparison between hard and soft fluxes of the source in Table 6, which is $F_{15-150 \text{ keV}}/F_{0.3-10 \text{ keV}} \approx 16$, indicating that the star could have been undetected by BAT during a flare.

An estimate for the distance to this object can be evaluated, as suggested in Rodriguez et al. (2010), assuming similarity with the active star II Peg (which has magnitude $R \sim 6.9$ and distance 40 pc; Monet et al. 2003; van Leeuwen 2007). We considered that 2PBC J0620.8–2932 has a USNO-A2.0 magnitude $R \sim 14.7$ and we consequently obtained the distance reported in Table 6, which is actually an upper limit since we considered $A_V \sim 0 \text{ mag}$ because we cannot determine the reddening along the source line of sight with the presently available information.

4.4. AGNs

The results for the extragalactic sources are reported in Tables 7, D.1, and D.2, where for each source we list fluxes, the classification, the estimated redshift, the luminosity distance (in Mpc), the Galactic colour excess, and the colour excess local to the AGN host.

We found that among 45 extragalactic objects, 27 have strong redshifted broad and narrow emission lines that are typical of type 1 AGNs (Figs. 4 and 5) and 18 have only strong and redshifted narrow emission lines that are typical of a type 2 AGN nature (see Figs. 6–9).

In our sample, we report the redshift value for most AGNs for the first time and most of them are in the range 0.004–0.294, that is, the AGNs of our sample are located in the local Universe ($z < 0.3$) except 2PBC J2010.3–2522, the QSO reported in Table 5 which is at redshift 0.828.

Among our AGN sample, 20 objects are intermediate type Sy 1.2–1.5 and 5 are Sy 1.9, whereas of the 18 type 2 AGNs, 14 are Seyfert 2 galaxies, one is a starburst galaxy (2PBC J1555.0–6225, Fig. 7), one is a LINER (2PBC J2238.9+4050, Fig. 8), and one is an X-ray bright optically normal galaxy (XBONG, Comastri et al. 2002) which displays absorption features only (2PBC J1332.1–7751, Fig. 9).

Table 6. Main observational results for the active star as identified in the present sample of 2PBC sources.

Object	H_α		R mag	d (pc)	L_X
	EW	Flux			
2PBC J0620.8–2932	0.8 ± 0.2	14.3 ± 2.5	~ 14.7	~ 1500	$108 (15\text{--}150)^C$ $6.81 (0.3\text{--}10)^X$

Notes. EWs are expressed in Å, line fluxes are in units of 10^{-15} erg cm^{-2} s^{-1} , X-ray luminosities are in units of 10^{31} erg s^{-1} , and the reference band (between round brackets) is expressed in keV. In the last column, the upper case letter indicates the satellite and/or the instrument with which the corresponding X-ray flux measurement was obtained (see text). ^(C) From Cusumano et al. (2010).

Table 7. Synoptic table containing the main results for the QSO identified in the present sample of 2PBC sources.

Object	$F_{[\text{OII}]}$	F_{MgII}	z	D_L (Mpc)	$E(B - V)_{\text{Gal}}$	L_X
2PBC J2010.3–2522	0.3 ± 0.1 [0.6 ± 0.2]	1.3 ± 0.1 [1.8 ± 0.3]	0.828	5234.4	0.164	$42.6 (15\text{--}150)^C$ $4.03 (0.3\text{--}10)^X$ $47.7 (14\text{--}195)^B$

Notes. Emission-line fluxes are reported both as observed and (between square brackets) corrected for the intervening Galactic absorption $E(B - V)_{\text{Gal}}$ along the object line of sight (from Schlegel et al. 1998). Line fluxes are in units of 10^{-15} erg cm^{-2} s^{-1} , X-ray luminosities are in units of 10^{45} erg s^{-1} , and the reference band (between round brackets) is expressed in keV. In the last column, the upper case letter indicates the satellite and/or the instrument with which the corresponding X-ray flux measurement was obtained. ^(C) From Cusumano et al. (2010) and ^(X) from *Swift*/XRT. ^(B) From Baumgartner et al. (2013). The typical error of the redshift measurement is ± 0.001 .

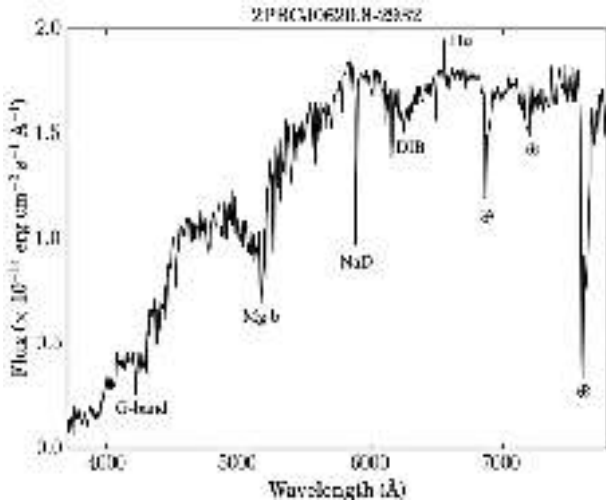


Fig. 3. Spectra (not corrected for the intervening Galactic absorption) of the optical spectra acquired for 2PBC J0620.8–2932, the optical counterpart of the active star belonging to the sample of BAT sources presented in this paper. For the spectrum, the main spectral features are labelled and ⊕ indicates telluric absorptions.

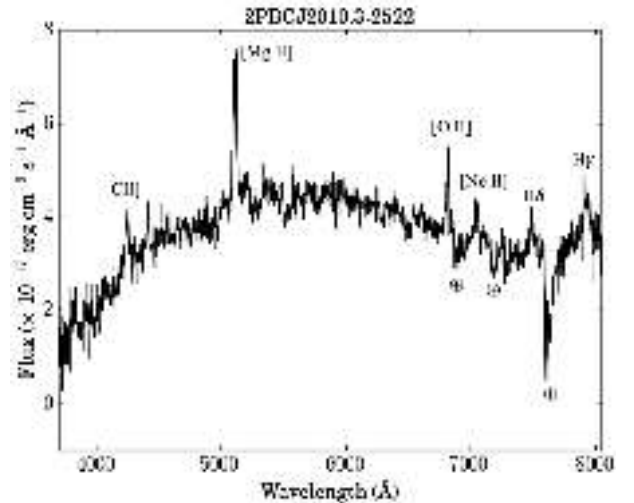


Fig. 4. Spectrum (not corrected for the intervening Galactic absorption) of the optical counterpart of the QSO belonging to the sample of BAT sources presented in this paper, 2PBC J2010.3–2522. For this spectrum, the main spectral features are labelled and ⊕ indicates telluric absorptions.

For type 1 AGNs, BH masses and Eddington luminosities are reported in Table D.3, where we corrected the measurement of the observed FWHM of H_β for the instrumental resolution corresponding to the relevant telescope setup (see Tables 2 and 3) in order to determine the BH masses. We only report the H_α emission for narrow line sources (Table D.2) as the H_α emission required more complex fits and sometimes had issues with the blending of [NII] emission lines and atmospheric lines.

For three Sy 2 objects, 2PBC J0356.6–6252, 2PBC J0608.0+5749, and 2PBC J2029.4–6146, $\left(\frac{F_{H\alpha}}{F_{H\beta}}\right)_*$ is less than 2.86, which implies that they could be type 2 AGN without local absorption (these are called “naked” Sy 2; Hawkins 2004). But, in particular, the object 2PBC J0356.6–6252 has strong IR emission due to dust according to Yamada et al. (2013), and the analysis of its X-ray spectra according to Ricci et al. (2015) indicates

a probably Compton thick nature, thus a more detailed study is needed to confirm the nature of this source.

As can be seen in Fig. 5, the spectrum of 2PBC J1548.5–3208 displays a composition of an AGN type Sy 1.9 at redshift 0.048 and a foreground star due to the inability of our setup to disentangle the pair of sources.

We note that for the object 2PBC J0819.2–2508, Cusumano et al. (2010) proposed a ROSAT soft X-ray counterpart in the catalogue (1RXS J081915.0–251106) and thus we acquired and analysed the spectrum of the optical object associated with the ROSAT source. However, we subsequently found in the XRT pointings of this field that the source analysed here has no emission above 3 keV; rather, there is another source inside the corresponding BAT error box of 2PBC J0819.2–2508 with emission above 3 keV (labelled as “XRT object” in Fig. A.4, left panel).

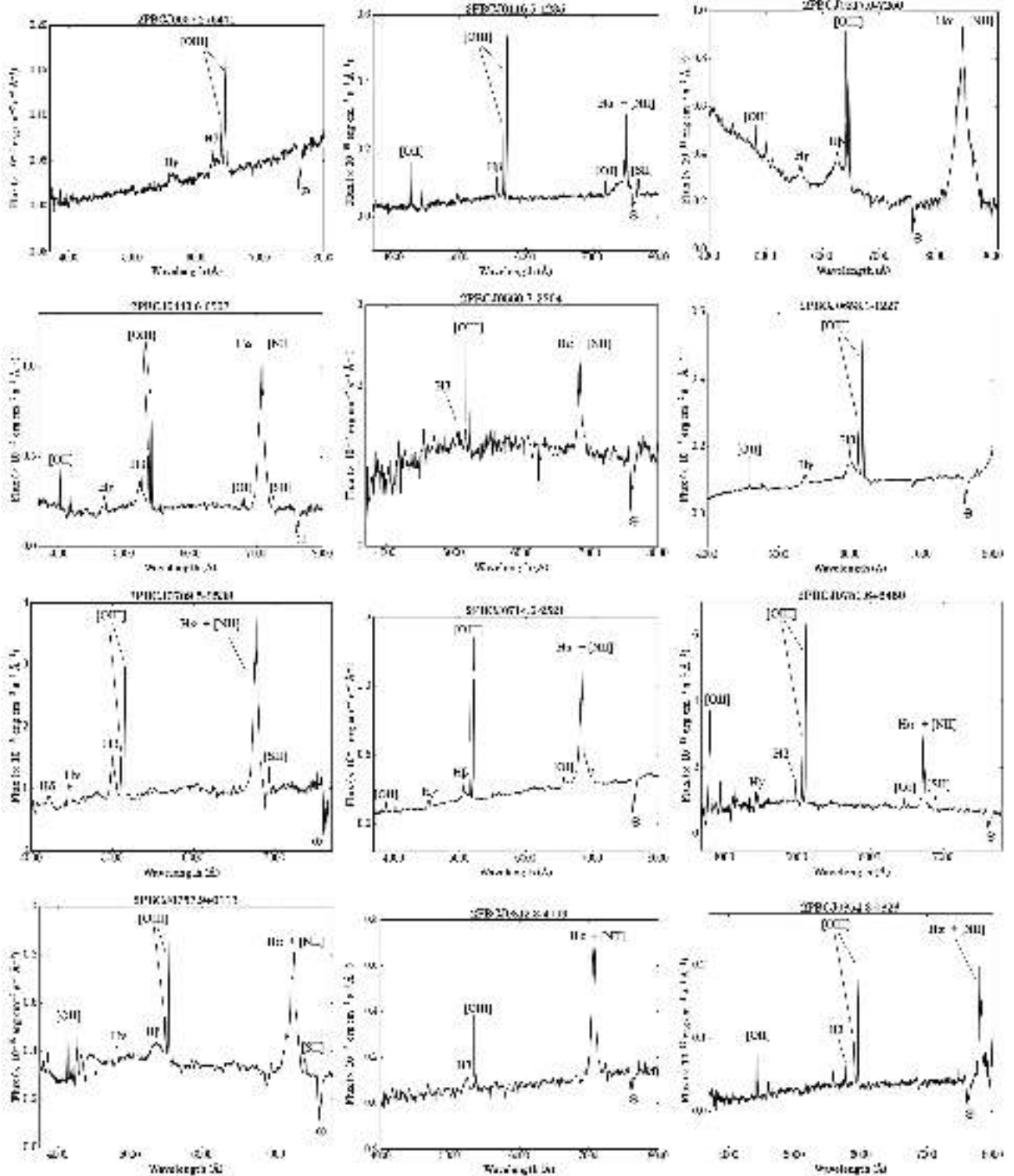


Fig. 5. Optical spectra of type 1 AGNs presented in this work (not corrected for the intervening galactic absorption). For each spectrum, the main spectral features are labelled and ⊕ indicates telluric absorptions.

This second source has coordinates (J2000) RA = 08:19:16.2, Dec = -25:07:06.9 with error radius of 6'' and is positionally associated with a $R \approx 19$ optical source. We think that the proposed ROSAT soft X-ray counterpart in Cusumano et al. (2010) could actually not be the real soft X-ray counterpart of 2PBC J0819.2-2508 and instead this other source could be; at the very least, both could be contributing to the detected hard X-ray

emission. The nature of this object and, in turn, an optical spectrum of this other source is required in order to confirm if this is a possible soft X-ray counterpart to 2PBC J0819.2-2508.

Similarly, the object 2PBC J1520.2-0433 has a proposed ROSAT soft X-ray counterpart in the Cusumano et al. (2010) catalogue, 1RXS J152017.4-043621 (see Fig. A.4 right panel, in magenta). We, however, found in the XRT observation of this

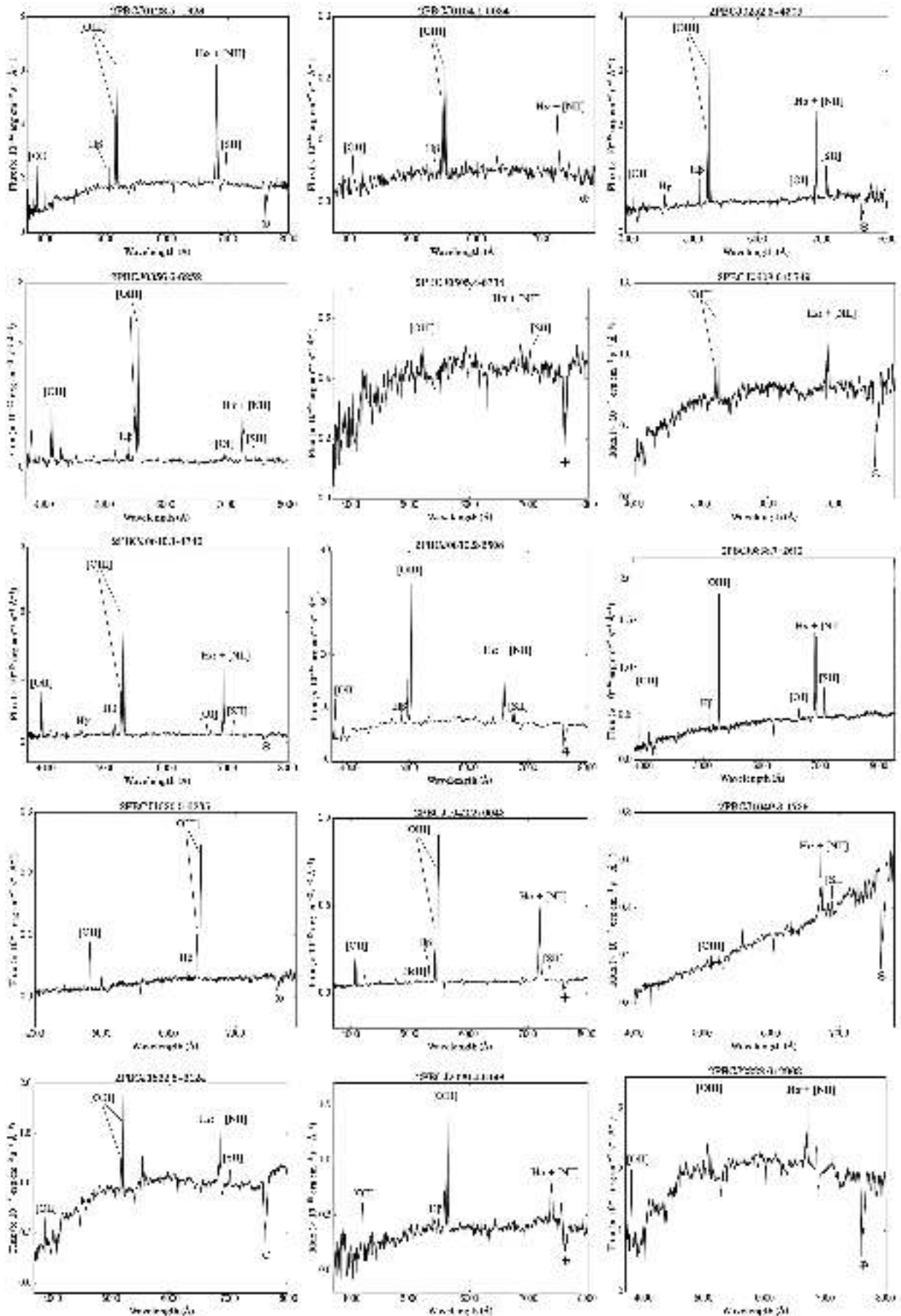


Fig. 6. Optical spectra of type 2 AGNs presented in this work (not corrected for the intervening galactic absorption).

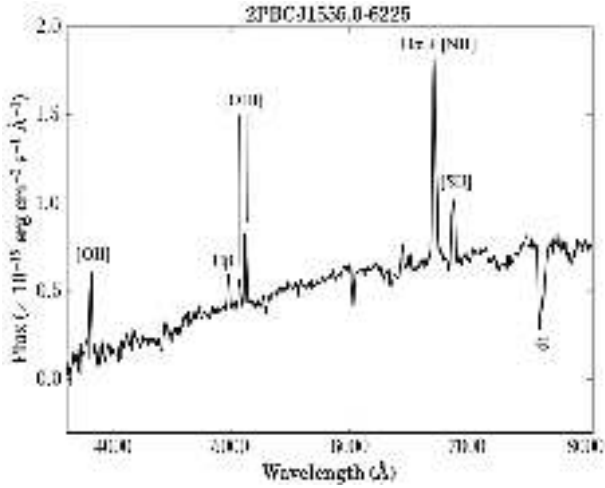


Fig. 7. Spectrum (not corrected for the intervening Galactic absorption) of the optical counterpart of the starburst galaxy belonging to the sample of BAT sources presented in this paper, 2PBC J1555.0-6225. For this spectrum, the main spectral features are labelled and \oplus indicates telluric absorptions.

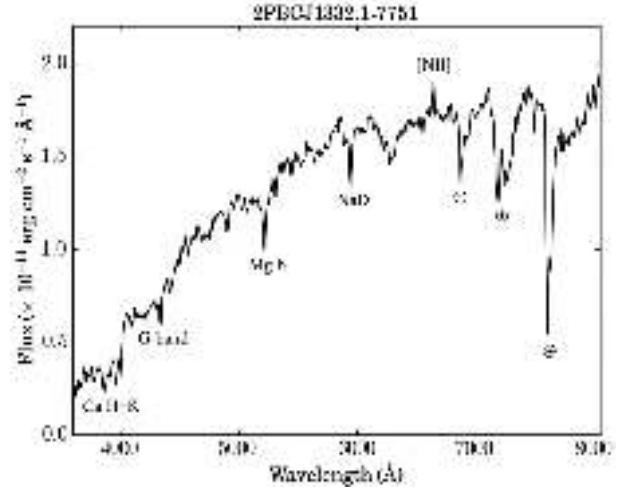


Fig. 9. Spectrum (not corrected for the intervening Galactic absorption) of the optical counterpart of the XBONG belonging to the sample of BAT sources presented in this paper, 2PBC J1332.1-7751. For this spectrum, the main spectral features are labelled and \oplus indicates telluric absorptions.

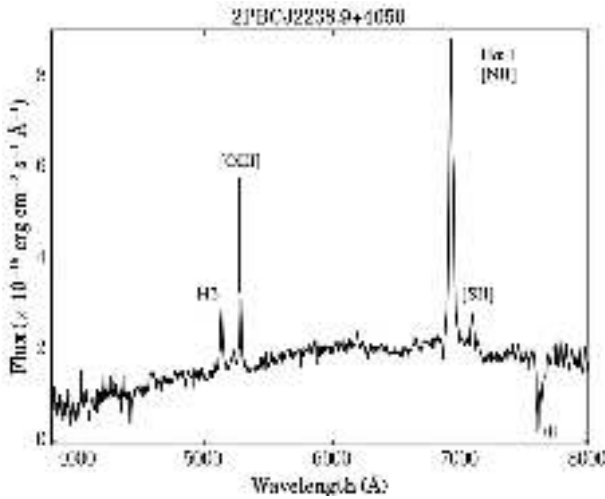


Fig. 8. Spectrum (not corrected for the intervening Galactic absorption) of the optical counterpart of the LINER belonging to the sample of BAT sources presented in this paper, 2PBC J2238.9+4050. For this spectrum, the main spectral features are labelled and \oplus indicates telluric absorptions.

field that this ROSAT source has no X-ray emission inside its error circle. Rather, there is another source inside the 90% BAT error circle of 2PBC J1520.2-0433, indicated with a black arrow in that figure, with emission above 3 keV. Thus, we considered this latter source as the actual soft X-ray counterpart for the optical follow-up.

As mentioned in Sect. 2, the object 2PBC J1020.5-0235 has two hard X-ray emitting sources just outside the 99% BAT error circle (see Fig. A.3), listed as Swift J1020.5-0237A and Swift J1020.5-0237B in the 70-month *Swift*-BAT catalogue of Baumgartner et al. (2013); in this work, we analysed the object A and we identified it as a Sy 2 at $z = 0.294$ (see Table D.2 and Fig. 6).

For the object 2PBC J2010.3-2522, that we classified as type 1 QSO at $z \sim 0.8$, we found in the literature that this object could be associated with a Fermi transient J2007-2518 that

is also spatially coincident with a radio source (Kocevski et al. 2014). Strader et al. (2014) acquired an optical spectrum of this same source and obtained results equivalent to ours. We thus confirm the QSO nature of this object and its possible association to the Fermi transient J2007-2518.

We found that the object classified as a starburst galaxy in our sample, 2PBC J1555.0-6225, has WISE magnitudes and colours that indicate an AGN nature according to the criteria of Secrest et al. (2015): $(W1 - W2) = 0.56$, $(W2 - W3) = 2.34 > 2$. This could be an elusive AGN as in Smith et al. (2014) and we are probably only seeing the starburst contribution in its optical spectrum, with the X-ray emission detected from the hidden nuclear activity.

For the object 2PBC J1332.1-7751, classified as XBONG, Davies et al. (2015) reported a column density in X-ray of $\text{Log}(N_{\text{H}}) = 23.8 \text{ cm}^{-2}$, that is almost at the limit to be a Compton Thick object (with $\text{Log}(N_{\text{H}}) \gtrsim 24 \text{ cm}^{-2}$) and they classified it as a Seyfert galaxy, but no optical classification is considered for this object in that work. Thus, 2PBC J1332.1-7751 is a peculiar object that is absorbed in X-ray and optically obscured. Our classification as XBONG is then supported by the information from Davies et al. (2015): the AGN optical appearance is likely hidden due to dust obscuration revealed in X-ray spectrum.

We note that in the field of the object 2PBC J0838.7+2612, there is another object with emission above 3 keV inside the 99% BAT error circle, indicated with tick marks (see Fig. A.1). For the sake of completeness, in Appendix B we thus report the main optical spectroscopic information we gathered about this source (a galaxy pair). Furthermore, the soft X-ray source that we associated with the object 2PBC J2030.7-7530 is the hardest source with emission above 3 keV within the BAT error circle (its count rate is at least 20 times larger than the other sources within the BAT error box). In the same way, the object 2PBC J1419.2+6804 has a count rate two orders of magnitude stronger than the other objects inside the 90% BAT error circle (see Appendix A).

We then looked for Compton-thick AGNs. In order to explore this nature, we applied the diagnostic T of Bassani et al. (1999), that is, the ratio of the measured 2-10 keV X-ray flux to the unabsorbed flux of the [OIII] λ 5007 forbidden emission line, to the objects which are classified as type 2 AGNs in our sample.

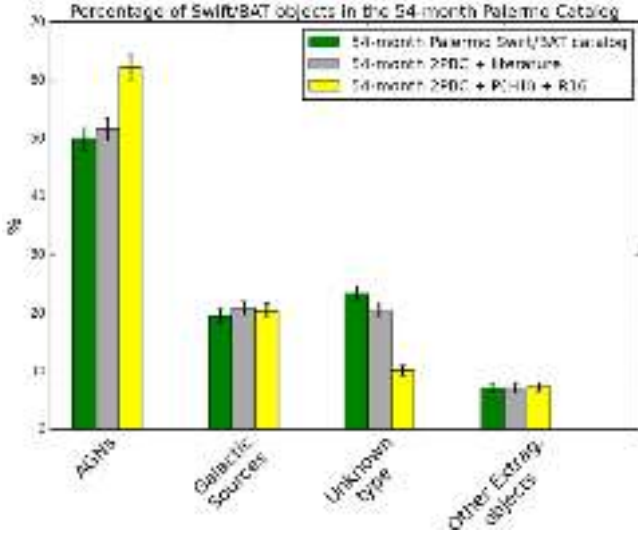


Fig. 10. Histogram, subdivided into source types, showing how the initial percentage of objects in the 54 months Palermo *Swift*-BAT catalogue (in green) has changed by means of the identifications performed by other authors (in grey) and by our group in PI-PIII and in this work (R16) (in yellow).

It was found that all objects show a T parameter >1 (from 2.5 to 430), so all of them apparently lie in the Compton thin regime, with $N_{\text{H}} < 10^{24} \text{ cm}^{-2}$. We, however, stress that the T values should be considered as upper limits because the soft X-ray fluxes that we considered refer to bands which are wider (0.3–10 keV) than the one for which this method should be applied (2–10 keV).

Moreover, we support this result by applying the criterion of Malizia et al. (2007): we found that all our type 2 AGNs lie in the Compton thin regime with softness ratio $F_{\text{X,soft}}/F_{\text{X,hard}}$ from 0.02 to 0.41. Although we use a different soft and hard X-ray ranges (0.3–10 keV and 15–150 keV instead of 2–10 keV and 20–100 keV), the approach can be considered equivalent and the results comparable.

4.5. Statistics

We here give an update of the statistics concerning the identifications of new hard X-ray *Swift*-BAT sources including the results of our group in this work and those in PI, PII, and PIII.

Considering all works, we identified 171 *Swift*-BAT objects through optical spectroscopy and their separation into the main classes is the following: 157 (92%) are AGNs, two are starburst galaxies (1%), one (0.6%) is probably an X-ray binary, ten (5.8%) are CVs, and one case (0.6%) is likely identified as an active star. We were able to drastically decrease the percentage of unidentified objects in the BAT survey, as shown in Fig. 10, where the unknown source type percentage decreased from more than 20% to $\sim 10\%$ thanks to our systematic work (yellow bars).

The green bars in Fig. 10 represent the initial 54-month Palermo *Swift*-BAT catalogue and the grey bars represent the classification of 20 AGNs and 18 galactic objects performed by other authors and available in the literature, as well as by our group using information already existing in the Simbad database (see Appendix C for the relevant information concerning these sources). We would like to stress that those other works have been able to reduce by $\sim 3\%$ the percentage of unclassified sources in the catalogue of Cusumano et al. (2010), whereas our

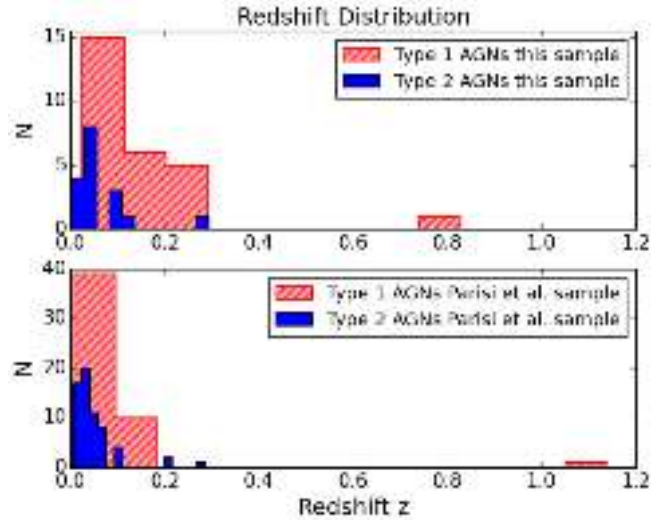


Fig. 11. Histograms showing the redshift distribution of *Swift*-BAT objects analysed and classified as AGNs in this sample (above) and those in the previous works of PI-III (below).

enduring classification work has allowed us to decrease by $\sim 10\%$ the percentage of these objects.

All AGNs (Seyfert 1, Seyfert 2, starburst galaxy, and LINERs) and XBONG in our sample and PI-PIII samples are at low redshifts ($z < 0.5$) while only two QSOs are located at $z > 0.5$.

We can see that the high-redshift QSOs found in our identification programme are of type 1. This is reasonably explained by the evidence that soft X-rays, needed for a precise localisation of the source, are not easily detected from type 2 QSOs due to local absorption in these sources, which adds to the faintness tied to their distance.

Figure 11 shows the redshift distribution of AGNs analysed in this work and the previous works of PI, PII, and PIII, represented by a histogram and binned according to the rules of Knuth (2006), which are based on the optimisation of a Bayesian fitness function across fixed-width bins.

The redshift distributions for the present sample and that of the PI-III merged sample were studied through a two sample Kolmogorov-Smirnov (KS) test. When we compare our redshift sample of Sy 1 with that of PI-III, we find that the KS test gives a p -value ~ 0.001 , whereas the comparison between the Sy 2 samples gives a p -value ~ 0.178 . This suggests that our Sy 1 sample is drawn from a different redshift distribution compared with the Sy 1 sample of PI-III. There is no univocal explanation for this: the difference could be due, for instance, to the fact that we on average used larger telescopes than those used in the PI-III works, thus we were able to observe fainter (and likely more distant) objects. On the other hand, when we compare the distributions of Sy 2 galaxies in the two samples, we see that they are consistent with belonging to the same parent population; therefore the above interpretation cannot be applied to this class of AGNs.

Moreover, we noted that the Sy 1 sample has on average a higher z (~ 0.130) than the Sy 2 sample (at $z \sim 0.066$). Interestingly the objects classified as naked Sy 2 are those few at higher z . This could explain why we see a difference with PI-III samples: indeed, in our selection of sources we are observing more distant Sy 1 galaxies, while this does not occur in the case of Sy 2 AGNs (except the naked ones) given that they are expected to be more absorbed and thus even fainter with distance

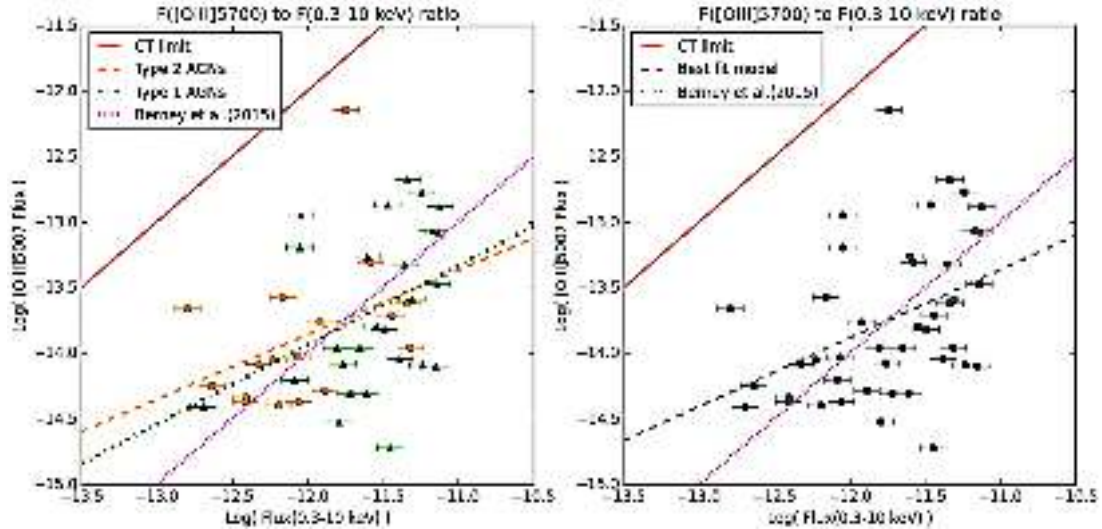


Fig. 12. Distribution of the [OIII] λ 5007 to 0.3–10 keV ratio for the AGNs of our sample and corresponding best-fit correlations (see text for details). Red continuous line represents the locus for which the parameter T is equal to 1 and the dotted pink line indicates the Berney et al. (2015) relation for the ratio between the soft X-ray flux and the [OIII] λ 5007 unabsorbed flux.

(which means they are difficult to observe with medium-sized telescopes).

Considering this work and PI-III, we found 12 Galactic objects: ten of these are CVs (i.e. 84% of the galactic identifications) and most of them are of magnetic type, whereas one object is an X-ray Binary, most probably a LXRIB (8%) and the remaining one is an active star (8%). We can confirm that the *Swift* satellite is efficient in detecting magnetic CVs because these objects are hard X-ray emitting sources due to their magnetic nature, and because the BAT surveys allow the study of objects outside the Galactic plane and, among them, hard X-ray emitting CVs.

We additionally tested the distribution of our AGNs by comparing the [OIII] λ 5007 unabsorbed flux with the soft X-ray flux following Berney et al. (2015). Specifically, we constructed a plot of the relative strength of the unabsorbed [OIII] λ 5007 emission line and the soft X-ray flux. It is important to stress that the soft X-ray fluxes considered refer to a wider band (0.3–10 keV) than that in Berney et al. (2015; 2–10 keV). So, these fluxes should conservatively be considered as upper limits. We found that when we compare the soft X-ray flux with that of the [OIII] λ 5007 emission line in our type 2 AGN sample, the relation between them shows a Pearson correlation coefficient of $R_{\text{Pear}} = 0.39$ and p -value = 0.13, with a standard deviation of ~ 0.50 dex. The plot of the relation is shown in Fig. 12 left panel, with the best fit model (slope 0.49 ± 0.09 , orange dashed line) and the locus for which the parameter T is equal to 1 (red continuous line). In this panel, we also show the best fit model for our type 1 AGNs, as a dash-dot line (with slope of 0.60 ± 0.09 , in green). We found that for this sample the Pearson correlation coefficient is $R_{\text{Pear}} = 0.37$ with a p -value = 0.06 and a standard deviation of ~ 0.55 dex. The dotted line (in pink) in both panels indicates the Berney et al. (2015) relation for the ratio between the soft X-ray flux and the [OIII] λ 5007 unabsorbed flux. Finally, in the right panel we compare the soft X-ray flux with that of the [OIII] λ 5007 emission line in our entire AGN sample (type 1 and type 2), with the best fit as a dashed line (with slope 0.52 ± 0.03 , in grey), finding a Pearson correlation coefficient of $R_{\text{Pear}} = 0.41$ with a p -value = 0.007 and a standard deviation of ~ 0.53 dex. We can see that the Berney et al. (2015) relation has a steeper slope than our fits. This is possibly due to the range of the soft

X-ray band we considered. Nevertheless, the results agree with those of Berney et al. (2015), suggesting to us that any correlation between these quantities, if present, is marginal at best.

5. Conclusions

In the present work, we identified and characterised 50 X-ray emitting objects with unknown or poorly explored natures, and which are listed in the 2PBC *Swift* survey. This was accomplished with the use of seven telescopes of different apertures, from 1.5 to 3.58 m, and of archival data from one spectroscopic survey.

Our main results are as follows.

- The majority of identifications are made up of extragalactic objects. Most of them are AGNs (26 are Seyferts of type 1, 15 cases are Seyferts of type 2, one is a LINER, one is a XBONG and one is a QSO of type 1) and one is a starburst galaxy. This confirms the trend of our previous findings that optical spectroscopy eminently enables the identification of hard X-ray emitting AGNs.
- In this work, we reported 30 new redshifts, 13 confirmations and two more accurate redshift values. All AGNs lie at redshift $z \lesssim 0.3$ except one of them, 2PBC J2010.3–2522, which is a QSO at $z \sim 0.8$. For most type 1 AGNs we estimated the BLR size, velocity, and the central BH mass as well as their Eddington ratio, and for type 2 AGNs we studied the local absorption.
- Our sample is thus dominated by extragalactic objects; among them we highlighted some peculiar objects, such as one galaxy displaying LINER features, one starburst galaxy, one XBONG, and two “naked” Seyfert 2 AGNs in the Compton thin regime.
- Five objects in our sample are galactic sources: one is probably a distant LXRIB, three are CVs of magnetic nature, and one is an active star.

This confirms the importance of this identification work on catalogued but unidentified high-energy sources, also because peculiar objects can be found within the considered samples (see MI-X and PI-III).

Surveys at optical and NIR wavelengths, such as the Vista Variables in the Vía Láctea (VVV; [Minniti et al. 2010](#); [Saito et al. 2012](#)) public NIR survey, will permit the identification of variable sources in the fields of the objects detected in published and forthcoming hard X-ray catalogues. This will facilitate the detection of putative NIR counterparts for these high-energy sources by means of accurate positional information and/or variability studies. In turn, this facilitates the detection of transient and persistent hard X-ray sources, especially in crowded fields such as those along the Galactic Plane and Bulge ([Rojas et al. 2012a,b, 2013](#); [Masetti et al. 2016](#); [Saito et al. 2016](#)).

Furthermore, the *NuSTAR* satellite ([Harrison et al. 2013](#)) with its high spatial resolution can allow the identification of blended sources such as the case of the object 2PBC J1548.5-3208 in our sample. Furthermore, thanks to its high energy resolution, *NuSTAR* can allow us to identify the different hard X-ray contributions of two sources in the same field, for example in the case of 2PBC J0819.2–2508, as demonstrated by [Koss et al. \(2016b\)](#) with *Swift* J2028.5+2543.

Acknowledgements. We thank Silvia Galletti for Service Mode observations at the Loiano telescope, and Roberto Gualandi, Ivan Bruni, and Antonio De Blasi for night assistance; Aldo Fiorenzano, Vania Lorenzi, and Walter Boschin for Service Mode observations at the TNG; Manuel Hernández, Rodrigo Hernández, and Jacqueline Seron for Service Mode observations at the CTIO telescope and Fred Walter for coordinating them. We thank the anonymous referee for useful comments and suggestions. We also acknowledge the use of public data from the *Swift* data archive. This work made use of data supplied by the UK *Swift* Science Data Centre at the University of Leicester, the ASI Science Data Center Multi-mission Archive, of the NASA Astrophysics Data System Abstract Service, the NASA/IPAC Extragalactic Database (NED), of the NASA/IPAC Infrared Science Archive, which are operated by the Jet Propulsion Laboratory, California Institute of Technology, under contract with the National Aeronautics and Space Administration, and of data obtained from the High Energy Astrophysics Science Archive Research Center (HEASARC), provided by NASA's GSFC. This publication made use of data products from the Two Micron All Sky Survey (2MASS), which is a joint project of the University of Massachusetts and the Infrared Processing and Analysis Center/California Institute of Technology, funded by the National Aeronautics and Space Administration and the National Science Foundation. This research has also made use of data extracted from the Sloan Digitized Sky Survey archive; the SIMBAD database operated at CDS, Strasbourg, France, and of the HyperLeda catalogue operated at the Observatoire de Lyon, France. Alejandra Rojas acknowledges financial support from Universidad Andrés Bello. Lorenzo Morelli acknowledges financial support from Padova University grant CPS0204. The IASF and IAPS co-authors acknowledge support from ASI/INAF agreement 2013.025.R0. Gaspar Galaz acknowledges the support of Basal center for Astrophysics and Technologies (CATA), PFB-06.

References

- Agudo, I., Bach, U., Krichbaum, T. P., et al. 2007, *A&A*, 476, L17
 Ajello, M., Rau, A., Greiner, J., et al. 2008, *ApJ*, 673, 96
 Aldcroft, T. L., Karovska, M., Cresitello-Dittmar, M. L., et al. 2000, in *X-ray Optics, Instruments, and Missions III*, eds. J. E. Truemper, & B. Aschenbach, *Proc. SPIE*, 4012, 650
 Altamirano, D., Linares, M., Patruno, A., et al. 2010, *MNRAS*, 401, 223
 Assafin, M., Andrei, A. H., Vieira Martins, R., et al. 2001, *ApJ*, 552, 380
 Baloković, M., Comastri, A., Harrison, F. A., et al. 2014, *ApJ*, 794, 111
 Barthelmy, S. D. 2004, *Proc. SPIE*, 5165, 175
 Bassani, L., Dadina, M., Maiolino, R., et al. 1999, *ApJS*, 121, 473
 Baumgartner, W. H., Tueller, J., Markwardt, C. B., et al. 2013, *ApJS*, 207, 19
 Berney, S., Koss, M., Trakhtenbrot, B., et al. 2015, *MNRAS*, 454, 3622
 Bird, A. J., Bazzano, A., Malizia, A., et al. 2016, *ApJS*, 223, 15
 Bikmaev, I. F., Burenin, R. A., Revnivtsev, M. G., et al. 2008, *Astron. Lett.*, 34, 653
 Buchanan, C. L., McGregor, P. J., Bicknell, G. V., & Dopita, M. A. 2006, *AJ*, 132, 27
 Butler, S. C., Tomsick, J. A., Chaty, S., et al. 2009, *ApJ*, 698, 502
 Burenin, R. A., Mescheryakov, A. V., Revnivtsev, M. G., et al. 2008, *Astron. Lett.*, 34, 367
 Burenin, R. A., Bikmaev, I. F., Revnivtsev, M. G., et al. 2009, *Astron. Lett.*, 35, 71
 Cardelli, J. A., Clayton, G. C., & Mathis, J. S. 1989, *ApJ*, 345, 245
 Casares, J., Zurita, C., Shahbaz, T., et al. 2004, *ApJ*, 613, L133
 Casares, J., Orosz, A., Zurita, C., et al. 2009, *ApJS*, 181, 238
 Coleiro, A., & Chaty, S. 2013, *ApJ*, 764, 185
 Coleiro, A., Chaty, S., Zurita Heras, J. A., et al. 2013, *A&A*, 560, A108
 Comastri, A., Mignoli, M., Ciliegi, P., et al. 2002, *ApJ*, 571, 771
 Cusumano, G., La Parola, V., Segreto, A., et al. 2010, *A&A*, 524, A64
 Davies, R. I., Burtscher, L., Rosario, D., et al. 2015, *ApJ*, 806, 127
 de Martino, D., Belloni, T., Falanga, M., et al. 2013, *A&A*, 550, A89
 Deutsch, E. W. 1999, *AJ*, 118, 1882
 Evans, P. A., Osborne, J. P., Beardmore, A. P., et al. 2014, *ApJ*, 210, 8
 Gehrels, N., Chincarini, G., Giommi, P., et al. 2004, *ApJ*, 611, 1005
 Gotthelf, E. V., Halpern, J. P., Terrier, R., & Mattana, F. 2011, *ApJ*, 729, L16
 Halpern, J. P., & Thorstensen, J. R. 2015, *AJ*, 150, 170
 Harrison, F. A., Craig, W. W., Christensen, F. E., et al. 2013, *ApJ*, 770, 103
 Hawkins, M. R. S. 2004, *A&A*, 424, 519
 Heckman, T. M. 1980, *A&A*, 87, 152
 Ho, L. C. 2009, *ApJ*, 699, 626
 Ho, L. C., Filippenko, A. V., & Sargent, W. L. W. 1993, *ApJ*, 417, 63
 Ho, L. C., Filippenko, A. V., & Sargent, W. L. W. 1997, *ApJS*, 112, 315
 Horan, D., & Weekes, T. C. 2004, *New Astron. Rev.*, 48, 527
 Horne, K. 1986, *PASP*, 98, 609
 Jonker, P. G., & Nelemans, G. 2004, *MNRAS*, 354, 355
 Kahabka, P., & Hilker, M. 2005, *A&A*, 435, 9
 Kaspi, S., Smith, P. S., Netzer, H., et al. 2000, *ApJ*, 533, 631
 Kauffmann, G., Heckman, T. M., Tremonti, C., et al. 2003, *MNRAS*, 346, 1055
 Klus, H., Bartlett, E. S., Bird, A. J., et al. 2013, *MNRAS*, 428, 3607
 Knuth, K. H. 2006, *ArXiv e-prints* [[arXiv:physics/0605197](#)]
 Kocevski, D., Ajello, M., Buehler, R., et al. 2014, *ATel*, 6553
 Koss, M. J., Assef, R., Baloković, M., et al. 2016a, *ApJ*, 825, 85
 Koss, M. J., Glidden, A., Baloković, M., et al. 2016b, *ApJ*, 824, L1
 Krivonos, R., Revnivtsev, M., Lutovinov, A., et al. 2007, *A&A*, 475, 775
 Landi, R., Masetti, N., Morelli, L., et al. 2007, *ApJ*, 669, 109
 Landi, R., Bassani, L., Dean, A. J., et al. 2009, *MNRAS*, 392, 630
 Landt, He., Cheung, C. C., & Healey, S. E. 2010, *MNRAS*, 408, 1103
 Lutovinov, A. A., Burenin, R. A., Revnivtsev, M. G., et al. 2012, *Astron. Lett.*, 38, 281
 Malizia, A., Landi, R., Bassani, L., et al. 2007, *ApJ*, 668, 81
 Malizia, A., Stephen, J. B., Bassani, L., et al. 2009, *MNRAS*, 399, 944
 Marconi, A., Risaliti, G., Gilli, R., et al. 2004, *MNRAS*, 351, 169
 Markwardt, C. B., Strohmayer, T. E., & Swank, J. H. 2008, *ATel*, 1443
 Masetti, N., Palazzi, E., Pian, E., et al. 2003, *A&A*, 404, 465
 Masetti, N., Palazzi, E., Bassani, L., et al. 2004, *A&A*, 426, L41 (MI)
 Masetti, N., Mason, E., Bassani, L., et al. 2006a, *A&A*, 448, 547 (MII)
 Masetti, N., Pretorius, M. L., Palazzi, E., et al. 2006b, *A&A*, 449, 1139 (MIII)
 Masetti, N., Bassani, L., Bazzano, A., et al. 2006c, *A&A*, 455, 11 (MIV)
 Masetti, N., Morelli, L., Palazzi, E., et al. 2006d, *A&A*, 459, 21 (MV)
 Masetti, N., Mason, E., Morelli, L., et al. 2008, *A&A*, 482, 113 (MVI)
 Masetti, N., Parisi, P., Palazzi, E., et al. 2009, *A&A*, 495, 121 (MVII)
 Masetti, N., Parisi, P., Palazzi, E., et al. 2010, *A&A*, 519, A96 (MVIII)
 Masetti, N., Parisi, P., Jiménez-Bailón, E., et al. 2012, *A&A*, 538, A123 (MIX)
 Masetti, N., Parisi, P., Palazzi, E., et al. 2013, *A&A*, 556, A120 (MX)
 Masetti, N., Saito, R. K., Rojas, A., & Minniti, D. 2016, *ATel*, 8733
 Minniti, D., Lucas, P. W., Emerson, J. P., et al. 2010, *New Astron.*, 15, 433
 McLure, R. J., & Jarvis, M. J. 2002, *MNRAS*, 337, 109
 Monet, D. G., Levine, S. E., Canzian, B., et al. 2003, *AJ*, 125, 984
 Morelli, L., Calvi, V., Masetti, N., et al. 2013, *A&A*, 556, A135
 Osterbrock, D. E. 1989, *Astrophysics of Gaseous Nebulae and Active Galactic Nuclei* (Mill Valley: Univ. Science Books)
 Pandey, J. C., Singh, K. P., Drake, S. A., & Sagar, R. 2005, *ApJ*, 130, 1231
 Parisi, P., Masetti, N., Jiménez-Bailón, E., et al. 2009, *A&A*, 507, 1345 (PI)
 Parisi, P., Masetti, N., Jiménez-Bailón, E., et al. 2012, *A&A*, 545, A101 (PII)
 Parisi, P., Masetti, N., Rojas, A. F., et al. 2014, *A&A*, 561, A67 (PIII)
 Predehl, P., & Schmitt, J. H. M. M. 1995, *A&A*, 293, 889
 Renaud, M., Marandon, V., Gotthelf, E. V., et al. 2010, *ApJ*, 716, 663
 Riaz, B., Gizis, J. E., & Harvin, J. 2006, *AJ*, 132, 866
 Ricci, C., Ueda, Y., Koss, M. J., et al. 2015, *ApJ*, 815, L13
 Rigby, J. R., Diamond-Stanic, A. M., & Aniano, G. 2009, *ApJ*, 700, 1878
 Rodríguez, J., Tomsick, J. A., Bodaghee, A., et al. 2009, *A&A*, 508, 889
 Rodríguez, J., Tomsick, J. A., & Bodaghee, A. 2010, *A&A*, 517, A14
 Roeser, S., Demleitner, M., & Schilbach, E. 2010, *AJ*, 139, 2440
 Rojas, A., Masetti, N., & Minniti, D. 2012a, *ATel*, 4006
 Rojas, A., Masetti, N., & Minniti, D. 2012b, *ATel*, 4342
 Rojas, A., Masetti, N., & Minniti, D. 2013, *ATel*, 4802
 Saito, R. K., Hempel, M., Minniti, D., et al. 2012, *A&A*, 537, A107
 Saito, R. K., da Silva, M. V., Melo, I. S., et al. 2016, *ATel*, 8456
 Scaringi, S., Bird, A. J., Norton, A. J., et al. 2010, *MNRAS*, 401, 2207
 Schlegel, D. J., Finkbeiner, D. P., & Davis, M. 1998, *ApJ*, 500, 525

- Secrest, N. J., Dudik, R. P., Dorland, B. N., et al. 2015, *ApJS*, **221**, 12
- Sguera, V., Bazzano, A., Bird, A. J., et al. 2006, *ApJ*, **646**, 452
- Sguera, V., Bazzano, A., Flocchi, M., et al. 2016, *ATel*, 9255
- Skrutskie, M. F., Cutri, R. M., Stiening, R., et al. 2006, *AJ*, **131**, 1163
- Smith, K. L., Koss, M., & Mushotzky, R. F. 2014, *ApJ*, **794**, 112
- Stephen, J. B., Bassani, L., Malizia, A., et al. 2006, *A&A*, **445**, 869
- Strader, J., Chomiuk, L., Landoni, M., et al. 2014, *ATel*, 6555
- Thorstensen, J. R., & Halpern, J. 2013, *AJ*, **146**, 107
- Ubertini, P., Lebrun, F., Di Cocco, G., et al. 2003, *A&A*, **411**, L131
- Ueda, Y., Hashimoto, Y., Ichikawa, K., et al. 2015, *ApJ*, **815**, 1
- van Leeuwen, F. 2007, *A&A*, **474**, 653
- van Paradijs, J., & McClintock, J. E. 1995, Optical and ultraviolet observations of X-ray binaries, in X-ray Binaries, eds. W. H. G. Lewin, J. van Paradijs, & E. P. J. van den Heuvel (Cambridge: Cambridge Univ. Press), 58
- Veilleux, S., & Osterbrock, D. E. 1987, *ApJS*, **63**, 295
- Vestergaard, M. 2004, Black-Hole Mass Measurements, in AGN Physics with the Sloan Digital Sky Survey, eds. G. T. Richards, & P. B. Hall (San Francisco: ASP), *ASP Conf. Ser.*, **311**, 69
- Voges, W., Aschenbach, B., Boller, T., et al. 1999, *A&A*, **349**, 389
- Warner, B. 1995, Cataclysmic variable stars (Cambridge: Cambridge University Press)
- Watson, M. G., Schröder, A. C., Fyfe, D., et al. 2009, *A&A*, **493**, 339
- Winkler, C., Courvoisier, T. J.-L., Di Cocco, G., et al. 2003, *A&A*, **411**, L1
- Winkler, H. 1992, *MNRAS*, **257**, 677
- Winter, L., Lewis, K. T., Koss, M., et al. 2010, *ApJ*, **710**, 503
- Wright, E. L. 2006, *PASP*, **118**, 1711
- Wu, X.-B., Wang, R., Kong, M. Z., et al. 2004, *A&A*, **424**, 793
- Yamada, R., Oyabu, S., Kaneda, H., et al. 2013, *PASJ*, **65**, 103
- Zurita Heras, J. A., Chaty, S., & Tomsick, J. A. 2009, *A&A*, **502**, 787

Appendix A: Finding charts of the new soft X-ray identifications

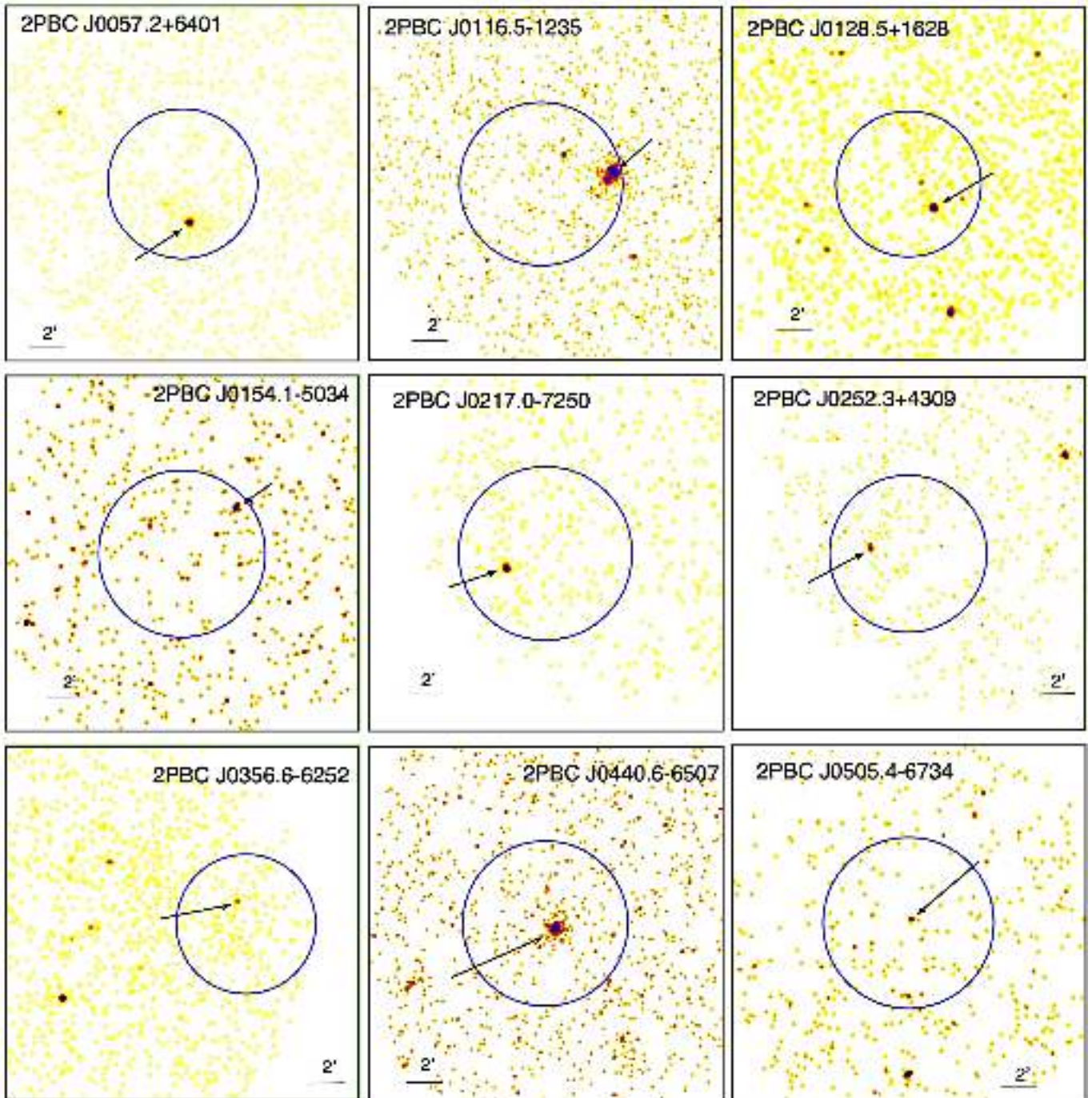


Fig. A.1. Soft X-ray images (0.3–10 keV) of the fields of 2PBC hard X-ray sources selected in this paper for optical spectroscopic follow-up. The object name is indicated in each panel. The BAT error circle is shown in blue and the new soft X-ray counterpart identifications for which the optical spectra were acquired are indicated with black arrows. In all cases, the objects selected as soft X-ray counterparts are the only ones with emission above 3 keV or with emission at 3σ considering the entire band of 0.3–10 keV. Field sizes are $20' \times 20'$. Nearly all images were extracted from the ASDC XRT database. In all cases, north is up and east to the left.

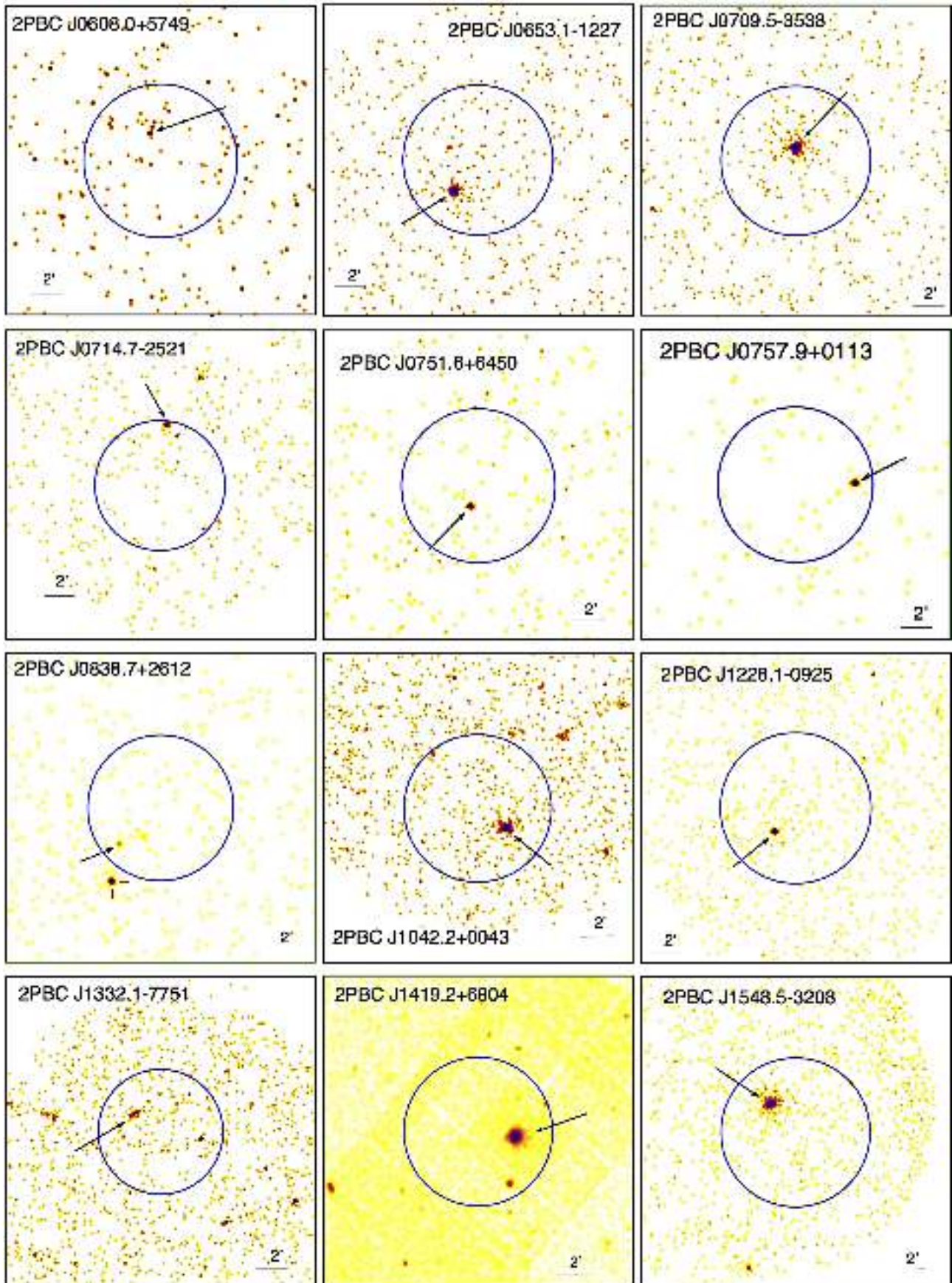


Fig. A.1. continued. The soft X-ray image of the field of 2PBC J1419.2+6804 was obtained from an *XMM-Newton* observation downloaded from the HEASARC database. In the field of the object 2PBC J0838.7+2612, there is another X-ray emitting object inside the 99% BAT error circle labelled with red tick marks.

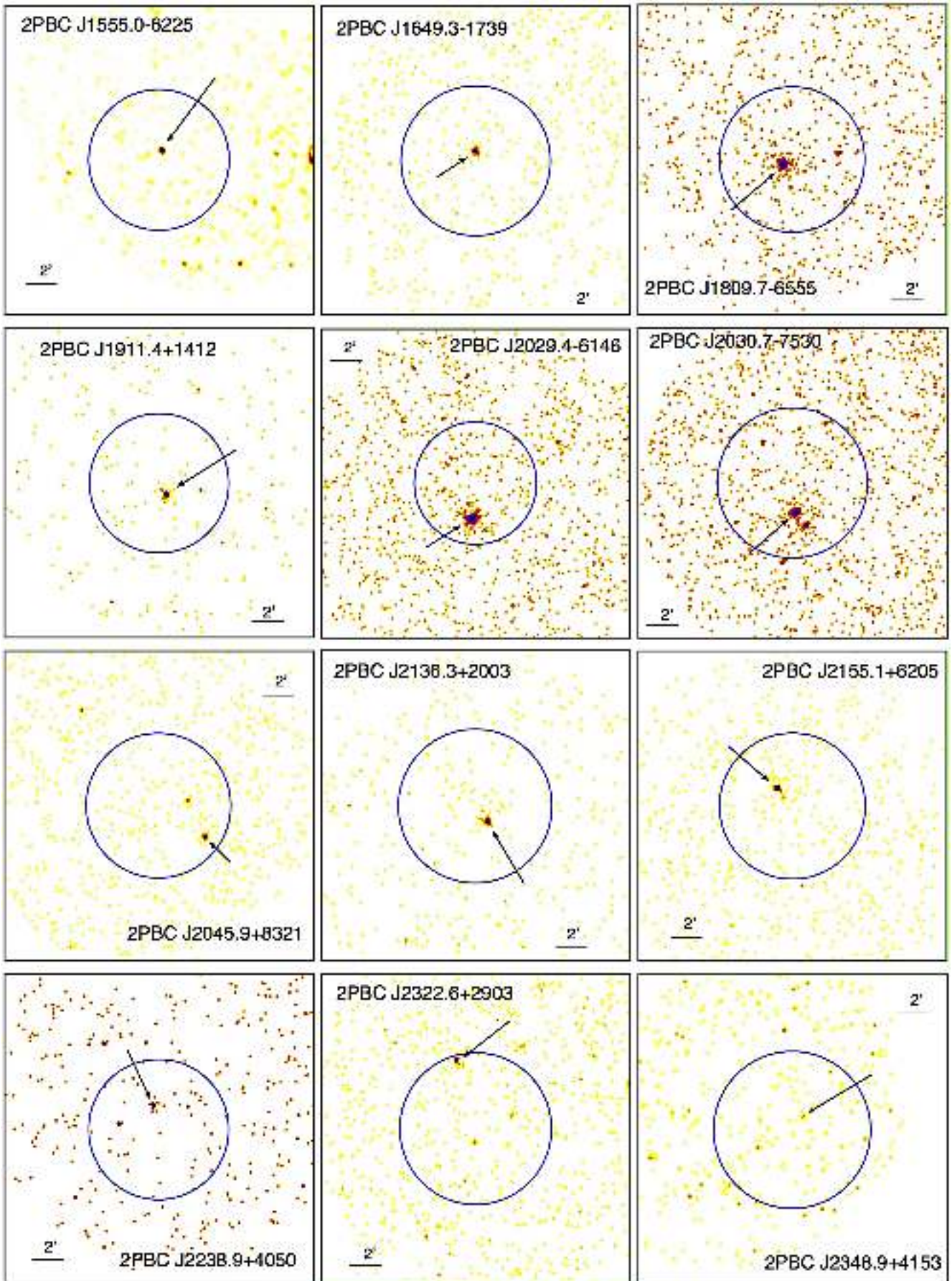


Fig. A.1. continued.

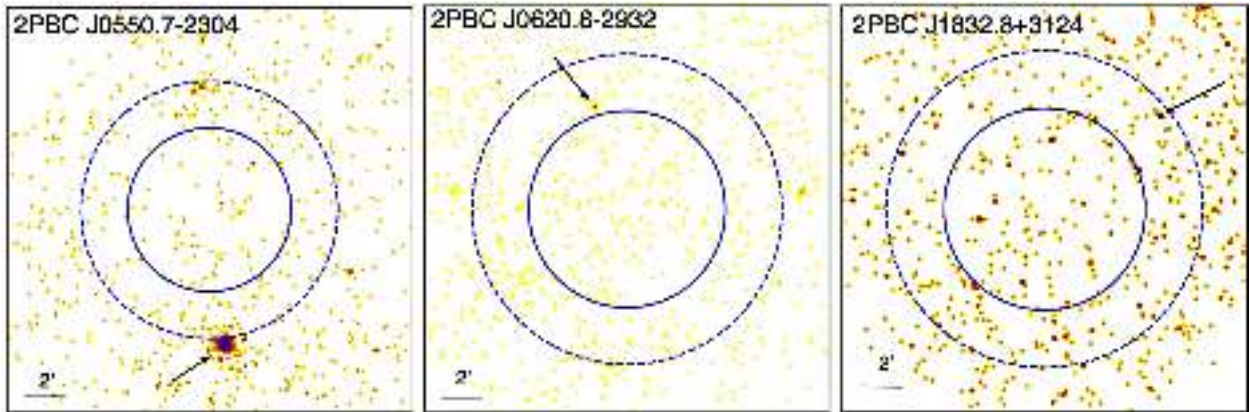


Fig. A.2. XRT soft X-ray images (0.3–10 keV) of the fields of *2PBC* sources for which the corresponding soft X-ray counterpart is outside the 90% error BAT circle (continuous circle, in blue) and inside or at the edge of the 99% BAT error circle, indicated with dashed blue line. The counterpart identifications for which the optical spectra were acquired are indicated with arrows. Field sizes are $20' \times 20'$. In all cases, north is up and east to the left.

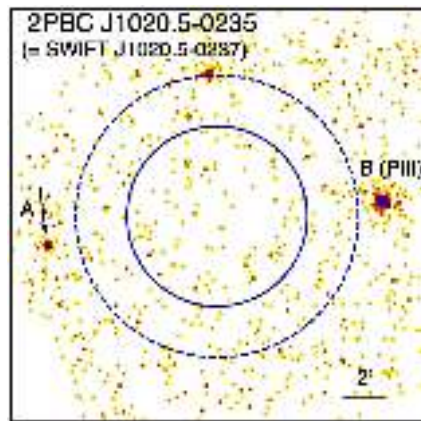


Fig. A.3. XRT soft X-ray observation of the field of *2PBC* J1020.5–0235. The 90% BAT error circle is shown as a continuous blue line while the 99% error circle is indicated with a dashed blue line. The object for which optical spectroscopy was acquired is indicated with an arrow. Information on object B is presented in PIII. Field size is $20' \times 20'$. North is up and east to the left.

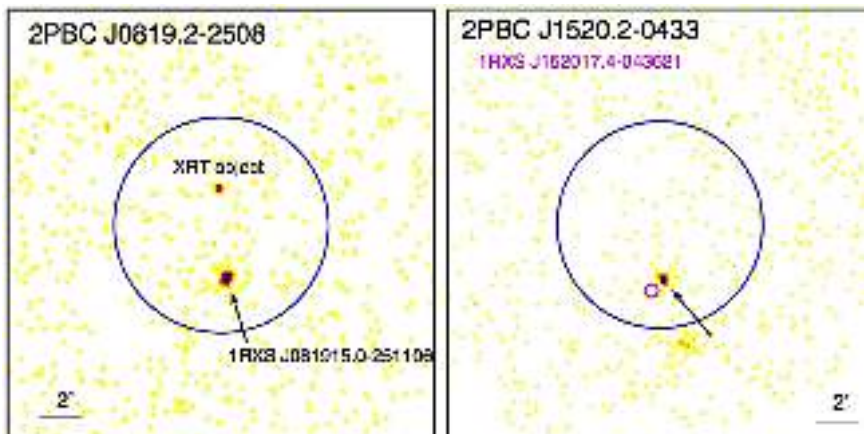


Fig. A.4. Soft X-ray observations (0.3–10 keV) of the field of two *2PBC* sources for which the positions of the soft X-ray counterparts proposed in this work do not coincide with those reported in the [Cusumano et al. \(2010\)](#) and/or [Baumgartner et al. \(2013\)](#) catalogues (see text). The 90% BAT error circle is shown in blue and our proposed soft X-ray counterpart identifications, for which the optical spectra were acquired, are indicated with arrows. Field sizes are $20' \times 20'$. In all cases, north is up and east to the left.

Appendix B: Extra X-ray emitting object in the field of 2PBC J0838.7+2612

As reported in the main text, we note that in the field of 2PBC J0838.7+2612 there is another object inside the 99% BAT error circle (labelled with red tick marks in Fig. A.3). This object has emission above 3 keV and is actually positionally coincident with two optical sources.

The spectra of these two objects were acquired on March 27, 2014 (UT start times at 22:29 and 22:49; exposure time of 2×1200 s) with the TNG Telescope in La Palma, Spain and

are presented in Fig. B.1; the information about the main optical properties of the LINER is reported in Table B.1.

We found that the pair of objects is composed of two galaxies at the same redshift $z = 0.048 \pm 0.001$ ($D_L = 229.7$ Mpc). One of them is a LINER and the other one is a normal galaxy; thus, we conclude that the LINER could be mainly responsible for the soft X-ray emission. We thus cannot exclude that the hard X-ray emission detected by BAT and labelled as 2PBC J0838.7+2612 in Cusumano et al. (2010) could partly be due to the LINER in this galaxy pair, albeit it nominally lies outside the 90% error circle of the BAT source.

Table B.1. Main results for the two additional X-ray emission objects observed in the field of 2PBC J0838.7+2612.

Optical coordinates (J2000)	$F_{H\alpha}$	$F_{H\beta}$	$F_{[OIII]}$	Class	z	D_L (Mpc)	$E(B-V)$		L_X
							Gal.	AGN	
RA = 08:38:59.29 Dec = +26:08:13.1	20.4 ± 3 [22.5 ± 4]	1.43 ± 0.15 [1.65 ± 0.12]	2.91 ± 0.12 [3.52 ± 0.3]	LINER	0.048	229.7	0.047	1.68	$1.74 (0.3-10)^X$

Notes. Optical coordinates were extracted from 2MASS catalogue, with an accuracy better than $\sim 0''.1$. Emission-line fluxes are reported both as observed and (between square brackets) corrected for the intervening Galactic absorption $E(B-V)_{Gal}$ along the object line of sight (from Schlegel et al. 1998). Line fluxes are in units of 10^{-15} erg cm^{-2} s^{-1} , X-ray luminosities are in units of 10^{43} erg s^{-1} , and the reference band (between round brackets) is expressed in keV. In the last column, ^(X) indicates that the luminosity was calculated using the corresponding X-ray flux measured from *Swift*/XRT counts rate assuming a power law model with photon index of $\Gamma = 1.8$. The typical error of the redshift measurement is ± 0.001 .

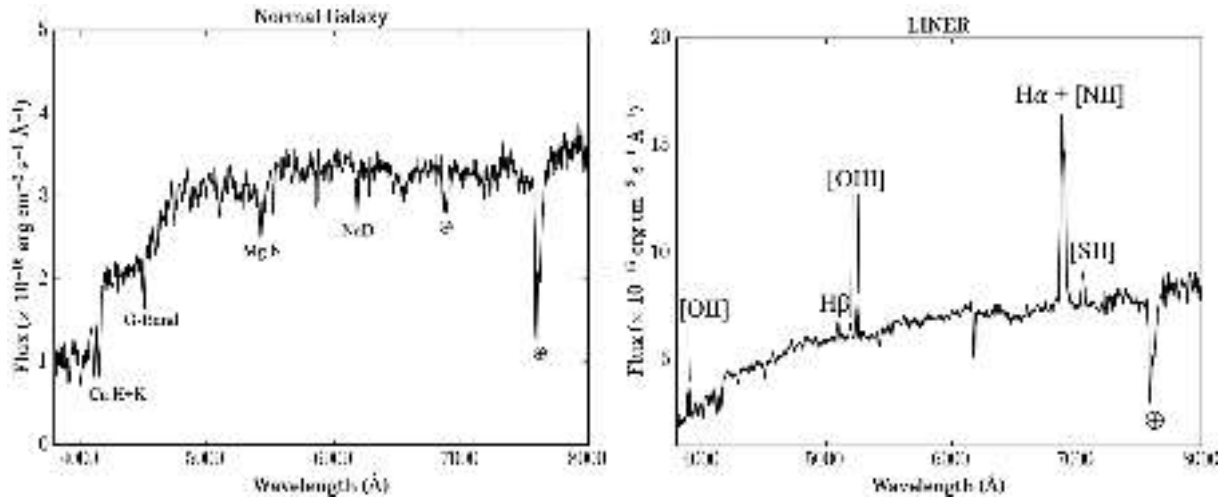


Fig. B.1. Optical spectra of the putative X-ray emitting objects in the field of 2PBC J0838.7+2612, both at the same redshift $z = 0.048$.

Appendix C: Information of the 54-month Palermo *Swift*-BAT catalogue from the literature and the Simbad database

Table C.1. Additional classification of 38 objects listed in the Cusumano et al. (2010).

Object ID	Class	Information
J0048.7+3157	Sy2	Simbad
J0207.0+2929	Sy1	Simbad
J0250.3+4645	Sy2	MX
J0325.1+4042	Sy2	MIX
J0328.7-2843	Sy2	Buchanan et al. (2006)
J0359.5+5058	QSO	Agudo et al. (2007)
J0547.3+5040	Sy2	MX
J0600.7+0008	QSO	Simbad
J0625.1+6450	Sy1	Simbad
J0712.1+1540	QSO	Simbad
J0823.0-0454	Sy2	Landi et al. (2007)
J0902.6-4813	Sy1	Zurita Heras et al. (2009)
J1105.8+5854	Sy1	Simbad
J1207.6+3353	Sy2	Landt et al. (2010)
J1213.0+3239	QSO	Simbad
J1346.5+1923	Sy1.2	MIX
J1414.2+1219	QSO	Simbad
J1745.7+2907	Sy1	Burenin et al. (2008)
J1826.0-0708	Sy1	Burenin et al. (2009)
J2021.7+4359	Sy2	Bikmaev et al. (2008)
J0207.9-7425	HXB	Kahabka & Hilker (2005)
J0451.1-6948	HXB	Klus et al. (2013)
J0537.7+2106	Star	Simbad
J0845.3-5227	Active star	Simbad
J1320.3-7013	Star	Riaz et al. (2006)
J1400.7-6323	SNR	Renaud et al. (2010)
J1632.7-4727	HXB	Coleiro et al. (2013)
J1711.8-3933	SNR	Horan & Weekes (2004)
J1735.4-3256	HXB	Coleiro et al. (2013)
J1747.2-2721	LXB	Altamirano et al. (2010)
J1758.5-2122	HXB	Coleiro et al. (2013)
J1810.3-1906	LXB	Markwardt et al. (2008)
J1821.4-1318	HXB	Butler et al. (2009)
J1848.8-0002	SNR	Gotthelf et al. (2011)
J1929.9+1818	HXB	Rodriguez et al. (2009)
J2218.4+1925	CV	Thorstensen & Halpern (2013)
J2337.7+4309	CV	Simbad
J2341.0+7642	CV	Lutovinov et al. (2012)

Notes. Classification of sources listed in the 54-month Palermo *Swift*-BAT catalogue performed by other authors and reported in the literature and/or Simbad database in Fig. 10 (grey bar). The extragalactic objects are shown in the upper part of the table, whereas the 18 galactic objects in the lower part.

Appendix D: Additional tables

Table D.1. Synoptic table containing the main results for the 26 low- z broad emission-line AGNs identified or observed in the present sample of 2PBC sources.

Object	$F_{H\beta}$	$F_{[OIII]}$	Class	z	D_L (Mpc)	$E(B-V)_{Gal}$	L_X
2PBC J0057.2+6401	5 ± 1 [62.3 \pm 5.2]	2.4 ± 0.1 [54.7 \pm 4.3]	Sy1.2	0.291	1499.1	1.252	2.15 (15–150) ^C 0.67 (0.3–10) ^X 2.7 (14–195) ^B
2PBC J0116.5–1235	0.8 ± 0.1 [0.7 \pm 0.1]	7.7 ± 0.1 [8.1 \pm 0.2]	Sy1.9	0.144	682.1	0.020	0.45 (15–150) ^C 0.32 (0.3–10) ^X 0.5 (14–195) ^B
2PBC J0217.0–7250	33 ± 1 [35 \pm 1]	14.8 ± 0.1 [16.1 \pm 0.1]	Sy1.2	0.291	1499.1	0.035	1.88 (15–150) ^C 0.77 (0.3–10) ^X
2PBC J0440.6–6507	16 ± 1 [18 \pm 1]	13.0 ± 0.1 [15.2 \pm 0.4]	Sy1.5	0.080	363.3	0.045	0.11 (15–150) ^C 0.05 (0.3–10) ^X
2PBC J0550.7–2304	12 ± 3 [18 \pm 6]	7.0 ± 0.7 [8.0 \pm 1.5]	Sy1.5	0.043	190.2	0.037	0.05 (15–150) ^C 0.03 (0.3–10) ^X
2PBC J0653.1–1227	7.7 ± 0.3 [45 \pm 6]	7.80 ± 0.02 [48.0 \pm 1.5]	Sy1.5	0.234	1169.1	0.861	1.31 (15–150) ^C 0.72 (0.3–10) ^X
2PBC J0709.5–3538	38.6 ± 2.5 [141 \pm 15]	24.6 ± 0.4 [85 \pm 1]	Sy1.5	0.030	131.4	0.401	0.02 (15–150) ^C 0.015 (0.3–10) ^X
2PBC J0714.6–2521	6.3 ± 2.5 [34.3 \pm 3.4]	13.5 ± 0.2 [64.1 \pm 0.7]	Sy1.5	0.042	185.6	0.512	0.04 (15–150) ^C 0.004 (0.3–10) ^X 0.08 (14–195) ^B
2PBC J0751.6+6450	7.5 ± 0.5 [8.6 \pm 0.5]	73.5 ± 0.8 [84 \pm 1]	Sy1.9	0.025	109.1	0.045	0.009 (15–150) ^C 0.002 (0.3–10) ^X
2PBC J0757.9+0113	14 ± 1 [17 \pm 1]	9.3 ± 0.7 [11 \pm 1]	Sy1.5	0.104	480.0	0.044	0.3 (15–150) ^C 0.061 (0.3–10) ^X
2PBC J0812.3–4003	3.6 ± 0.3 [461 \pm 78]	1.6 ± 0.2 [172 \pm 8]	Sy1.2	0.076	344.1	1.632	0.1 (15–150) ^C 0.08 (0.3–10) ^X 0.2 (14–195) ^B
2PBC J0854.3–0826	0.3 ± 0.1 [0.3 \pm 0.2]	2.80 ± 0.03 [3.0 \pm 0.1]	Sy1.9	0.189	920.2	0.032	0.8 (15–150) ^C 0.16 (0.3–10) ^X 1.3 (14–195) ^B
2PBC J1228.1–0925	197 ± 37 [183 \pm 56]	104 ± 6 [113 \pm 10]	Sy1.5	0.223	1107.3	0.036	1.47 (15–150) ^C 0.13 (0.3–10) ^X
2PBC J1251.8–5127	21.8 ± 1.2 [34 \pm 5]	15.0 ± 0.1 [26 \pm 5]	Sy1.5	0.178	861.0	0.201	0.9 (15–150) ^C 0.43 (0.3–10) ^X
2PBC J1419.2+6804	–	1.7 ± 0.2 [1.9 \pm 0.2]	likely Sy1.9	0.077	348.9	0.035	0.1 (15–150) ^C 0.05 (0.2–12) ^N
2PBC J1520.2–0433	96 ± 1 [134 \pm 1]	98 ± 1 [135 \pm 1]	Sy1.5	0.111	514.7	0.113	0.2 (15–150) ^C 0.11 (0.3–10) ^X
2PBC J1548.5–3208	–	22.5 ± 3.4 [34 \pm 5]	likely Sy1.9	0.048	213.1	0.109	0.04 (15–150) ^C 0.04 (0.3–10) ^X
2PBC J1709.7–2349	63 ± 13 [392 \pm 37]	18 ± 2 [86 \pm 10]	Sy1.2	0.036	158.4	0.536	0.03 (15–150) ^C 0.02 (0.2–12) ^N
2PBC J1742.0–6053	93.4 ± 8.4 [110 \pm 10]	109 ± 10 [132 \pm 10]	Sy1.5	0.152	723.6	0.077	0.6 (15–150) ^C 0.47 (0.3–10) ^X 0.7 (14–195) ^B
2PBC J1809.7–6555	–	6.8 ± 2.5 [9 \pm 3]	Sy1.5	0.181	877.0	0.067	0.7 (15–150) ^C 0.38 (0.3–10) ^X
2PBC J2030.7–7530	138 ± 11 [161 \pm 17]	168 ± 10 [213 \pm 10]	Sy1.5	0.114	529.6	0.088	0.3 (15–150) ^C 0.15 (0.3–10) ^X 0.4 (14–195) ^B
2PBC J2045.9+8321	3.4 ± 0.6 [3.8 \pm 0.6]	4.5 ± 0.1 [6.3 \pm 0.2]	Sy1.5	0.283	1451.9	0.142	1.26 (15–150) ^C 0.21 (0.3–10) ^X
2PBC J2048.3+3812	1.1 ± 0.5 [16.3 \pm 0.5]	0.4 ± 0.1 [5.0 \pm 0.1]	Sy1.2	0.106	489.9	0.890	0.2 (15–150) ^C 0.05 (0.3–10) ^X 0.2 (14–195) ^B
2PBC J2136.3+2003	27.0 ± 0.2 [37 \pm 1]	2.0 ± 0.4 [5 \pm 2]	Sy1	0.081	368.1	0.113	0.1 (15–150) ^C 0.04 (0.3–10) ^X
2PBC J2155.1+6205	1.4 ± 0.1 [14 \pm 1]	1.2 ± 0.1 [11 \pm 1]	Sy1.5	0.058	259.3	0.754	0.05 (15–150) ^C 0.012 (0.3–10) ^X
2PBC J2348.9+4153	7.2 ± 0.3 [9.6 \pm 0.3]	2.9 ± 0.1 [3.9 \pm 0.1]	Sy1.2	0.183	887.8	0.112	0.4 (15–150) ^C 0.02 (0.3–10) ^X

Notes. Emission-line fluxes are reported both as observed and (between square brackets) corrected for the intervening Galactic absorption $E(B-V)_{Gal}$ along the object line of sight (from [Schlegel et al. 1998](#)). Line fluxes are in units of 10^{-15} erg cm $^{-2}$ s $^{-1}$, X-ray luminosities are in units of 10^{45} erg s $^{-1}$, and the reference band (between round brackets) is expressed in keV. In the last column, the upper case letter indicates the satellite and/or the instrument with which the corresponding X-ray flux measurement was obtained. ^(C) From *Swift*-BAT, [Cusumano et al. \(2010\)](#). ^(B) From *Swift*-BAT, [Baumgartner et al. \(2013\)](#). ^(X) From *Swift*/XRT. ^(N) From *XMM-Newton*. The typical error of the redshift measurement is ± 0.001 .

Table D.2. Synoptic table containing the main results for the 18 narrow emission-line AGNs observed in the present sample of 2PBC sources.

Object	$F_{H\alpha}$	$F_{H\beta}$	$F_{[\text{OIII}]}$	Class	z	D_L (Mpc)	$E(B-V)$		L_X
							Gal.	AGN	
2PBC J0128.5+1628	59 ± 1 [68 \pm 2]	9.0 ± 0.7 [11 \pm 1]	78 ± 1 [93 \pm 1]	Sy2	0.038	167.5	0.062	0.82	4.03(15–150) ^C 0.29 (0.3–10) ^X 4.9 (14–195) ^B
2PBC J0154.1–5034	1.7 ± 0.1 [1.7 \pm 0.1]	0.6 ± 0.2 [0.6 \pm 0.2]	4.0 ± 0.1 [4.3 \pm 0.1]	Sy 2	0.101	465.2	0.017	~0.04	20.70 (15–150) ^C 1.0 (0.3–10) ^X
2PBC J0252.3+4309	19.3 ± 0.3 [24 \pm 1]	4.9 ± 0.3 [6.3 \pm 0.3]	34.8 ± 0.1 [46 \pm 1]	Sy2	0.051	226.9	0.093	0.27	7.39 (15–150) ^C 0.24 (0.3–10) ^X 8.04 (14–195) ^B
2PBC J0356.6–6252	15.7 ± 0.3 [17 \pm 5]	5.7 ± 0.4 [6.1 \pm 0.6]	49.8 ± 0.3 [56 \pm 1]	”Naked” Sy2	0.107	494.8	0.039	~0.0	29.3 (15–150) ^C 0.67 (0.3–10) ^X 36.1 (14–195) ^B
2PBC J0505.4–6734	–	–	2.5 ± 0.3 [5.2 \pm 0.6]	likely Sy2	0.046	203.9	0.229	–	3.48 (15–150) ^C 0.65 (0.2–12) ^N 5.9 (14–195) ^B
2PBC J0608.0+5749	1.5 ± 0.4 [4.9 \pm 0.4]	<3 [<5]	6.7 ± 0.3 [8.9 \pm 0.3]	”Naked” Sy2	0.050	222.3	0.099	~0.0	5.91 (15–150) ^C 0.35 (0.3–10) ^X
2PBC J0640.1–4740	17.7 ± 0.1 [21.9 \pm 0.1]	5.5 ± 0.6 [7.1 \pm 0.6]	36.5 ± 0.3 [50 \pm 1]	Sy2	0.056	250.0	0.099	0.13	6.73 (15–150) ^C 1.92 (0.3–10) ^X 10.3 (14–195) ^B
2PBC J0819.2–2508	193 ± 2 [272 \pm 10]	25 ± 4 [40 \pm 10]	453 ± 12 [719 \pm 12]	Sy2	0.004	17.2	0.145	0.876	0.02 (15–150) ^C 0.006 (0.3–10) ^X
2PBC J0838.7+2612	7.8 ± 0.1 [9 \pm 1]	0.8 ± 0.1 [0.9 \pm 0.2]	7.2 ± 0.1 [8.3 \pm 0.1]	Sy2	0.052	231.5	0.048	1.220	6.41 (15–150) ^C 0.30 (0.3–10) ^X
2PBC J1020.5–0235	–	0.2 ± 0.1 [0.3 \pm 0.1]	3.9 ± 0.1 [4.3 \pm 0.1]	Sy2	0.294	1517.0	0.042	–	303.0 (15–150) ^C 23.8 (0.3–10) ^X 194.7 (14–195) ^B
2PBC J1042.2+0043	8.2 ± 0.2 [9.3 \pm 0.2]	1.9 ± 0.1 [2.3 \pm 0.1]	16.6 ± 0.2 [19.5 \pm 0.2]	Sy2	0.096	440.7	0.056	0.350	23.2 (15–150) ^C 8.36 (0.3–10) ^X 28.2 (14–195) ^B
2PBC J1332.1–7751	–	–	–	XBONG	0.009	38.8	0.210	–	0.25 (15–150) ^C 0.02 (0.3–10) ^X 0.3 (14–195) ^B
2PBC J1555.0–6225	27.8 ± 4.1 [52 \pm 5]	4.1 ± 0.1 [10.0 \pm 0.3]	7.3 ± 0.3 [17.1 \pm 0.4]	likely Starburst Galaxy	0.022	95.8	0.271	0.599	1.1 (15–150) ^C 0.13 (0.3–10) ^X
2PBC J1649.3–1739	1.3 ± 0.1 [11 \pm 3]	–	0.6 ± 0.1 [11 \pm 2]	type 2 AGN	0.023	100.2	0.938	–	1.68 (15–150) ^C 0.58 (0.3–10) ^X
2PBC J1832.8+3124	10.1 ± 0.6 [13 \pm 1]	–	15.9 ± 0.7 [22 \pm 1]	Sy2	0.043	190.2	0.116	–	2.60 (15–150) ^C 0.07 (0.3–10) ^X
2PBC J2029.4–6146	6.5 ± 1.5 [8 \pm 3]	1.9 ± 0.1 [3.4 \pm 0.2]	21.0 ± 0.1 [24.0 \pm 0.1]	”Naked” Sy2	0.124	579.9	0.052	~0.0	44.3 (15–150) ^C 18.5 (0.3–10) ^X 63.6 (14–195) ^B
2PBC J2238.9+4050	14.9 ± 0.2 [28 \pm 7]	3.4 ± 0.2 [7.2 \pm 0.6]	2.0 ± 0.1 [4.0 \pm 0.4]	LINER	0.055	245.4	0.242	0.296	5.04 (15–150) ^C 0.46 (0.3–10) ^X
2PBC J2322.6+2903	6.5 ± 0.2 [8.9 \pm 0.2]	–	16.8 ± 0.4 [26.7 \pm 0.4]	Sy2	0.019	82.6	0.154	–	0.74 (15–150) ^C 0.06 (0.3–10) ^X

Notes. Emission-line fluxes are reported both as observed and (between square brackets) corrected for the intervening Galactic absorption $E(B-V)_{\text{Gal}}$ along the object line of sight (from Schlegel et al. 1998). Line fluxes are in units of 10^{-15} erg cm⁻² s⁻¹, X-ray luminosities are in units of 10^{43} erg s⁻¹, and the reference band (between round brackets) is expressed in keV. In the last column, the upper case letter indicates the satellite and/or the instrument with which the corresponding X-ray flux measurement was obtained. ^(C) From *Swift*-BAT, Cusumano et al. (2010). ^(B) From *Swift*-BAT, Baumgartner et al. (2013). ^(X) From *Swift*/XRT. ^(N) From *XMM-Newton*. The typical error of the redshift measurement is ± 0.001 .

Table D.3. BLR gas velocities (in km s^{-1}), central black hole masses (in units of $10^8 M_{\odot}$), Eddington luminosity, and apparent Eddington ratios for broad line AGNs discussed in this paper.

Object	v_{BLR}	M_{BH}	L_{Edd}	$L_{\text{BOL}}/L_{\text{Edd}}$
2PBCJ0057.2+6401	5803	11	136	0.09
2PBCJ0217.0–7250	10622	25	308	0.04
2PBCJ0440.6–6507	5046	0.5	6.4	0.10
2PBCJ0550.7–2304	2550	0.1	0.7	0.44
2PBCJ0653.1–1227	5184	5	62	0.12
2PBCJ0709.5–3538	2986	0.2	2.3	0.05
2PBCJ0714.6–2521	4086	0.2	2.6	0.09
2PBCJ0757.9+0113	9241	2.4	30	0.06
2PBCJ0812.3–4003	3229	1.8	22	0.03
2PBCJ1228.1–0925	16600	123	1542	0.01
2PBCJ1251.8–5127	6732	4.5	57	0.09
2PBCJ1520.2–0433	2937	1.1	14	0.09
2PBCJ1709.7–2349	1180	0.1	1.0	0.19
2PBCJ1742.0–6053	7895	11	138	0.03
2PBCJ2030.7–7530	4076	2.5	31	0.06
2PBCJ2045.9+8321	2325	0.2	3.1	2.41
2PBCJ2048.3+3812	11448	3.7	46	0.03
2PBCJ2136.3+2003	4501	0.7	8.4	0.07
2PBCJ2155.1+6205	2475	0.1	0.8	0.36
2PBCJ2348.9+4153	2373	0.2	3.1	0.76
2PBC J2010.3–2522	1575	1.3	16	15.4

Notes. The final uncertainties on the black hole mass estimates are about 50% of their values. The velocities were determined using $\text{H}\beta$ emission or Mg II (upper and lower part of the table, respectively), whereas the apparent Eddington luminosity (in units of $10^{45} \text{ erg s}^{-1}$) and ratios were computed using the bolometric luminosity obtained from the (observed or rescaled, see text) 15–150 keV luminosities.